MISCELLANEOUS PAPER HL-81-5

SIGNIFICANT STRESSES OF ARRESTED SALINE WEDGES

by

Garbis H. Keulegan

Hydraulics Laboratory
U. S. Army Engineer Waterways Experiment Station
P. O. Box 631, Vicksburg, Miss. 39180

August 1981

Final Report

Approved For Public Release; Distribution Unlimited

Prepared for Office, Chief of Engineers, U. S. Army
Washington, D. C. 20314

W34m
no. HL-81-5
c.4

Unclassified

SECURITY CLASSIFICATION OF THIS PAGE (When Data Entered)

REPORT DOCUMENTATION PAGE		READ INSTRUCTIONS BEFORE COMPLETING FORM
1. REPORT NUMBER Miscellaneous Paper HL-81-5	2. GOVT ACCESSION NO.	3. RECIPIENT'S CATALOG NUMBER
4. TITLE (and Subtitle) SIGNIFICANT STRESSES OF ARRESTED SALINE WEDGES		5. TYPE OF REPORT & PERIOD COVERED Final report
		6. PERFORMING ORG. REPORT NUMBER
7. AUTHOR(s) Garbis H. Keulegan		8. CONTRACT OR GRANT NUMBER(s)
9. PERFORMING ORGANIZATION NAME AND ADDRESS U. S. Army Engineer Waterways Experiment Station Hydraulics Laboratory P. O. Box 631, Vicksburg, Miss. 39180		10. PROGRAM ELEMENT, PROJECT, TASK AREA & WORK UNIT NUMBERS
11. CONTROLLING OFFICE NAME AND ADDRESS Office, Chief of Engineers, U. S. Army Washington, D. C. 20314		12. REPORT DATE August 1981
		13. NUMBER OF PAGES 88
14. MONITORING AGENCY NAME & ADDRESS(if different from Controlling Office)		15. SECURITY CLASS. (of this report) Unclassified
		15a. DECLASSIFICATION/DOWNGRADING SCHEDULE

16. DISTRIBUTION STATEMENT (of this Report)

Approved for public release; distribution unlimited.

17. DISTRIBUTION STATEMENT (of the abstract entered in Block 20, if different from Report)

18. SUPPLEMENTARY NOTES

Available from National Technical Information Service, 5285 Port Royal Road, Springfield, Va. 22151.

19. KEY WORDS (Continue on reverse side if necessary and identify by block number)

Fresh water
Salt water
Salt water-fresh water interfaces
Salt water intrusion

20. ABSTRACT (Continue on reverse side if necessary and identify by block number)

The hydrodynamical relations for the fresh water above and the arrested saline wedge below the interface are developed with a view toward evaluating the average interfacial stress and the average bottom stress along the entire length of the wedge. The relations are also verified by applying the principle of momentum separately to the fresh water and next to the saline wedge. Stresses are evaluated for arrested wedges observed in a laboratory channel, the densimetric Froude number falling close to 0.40. It is
(Continued)

DD FORM 1473, 1 JAN 73 EDITION OF 1 NOV 65 IS OBSOLETE

Unclassified

SECURITY CLASSIFICATION OF THIS PAGE (When Data Entered)

20. ABSTRACT (Continued).

found that the interfacial stresses are of viscous origin and are not modified in the cases when unilateral mixing is present.

PREFACE

The study reported herein was completed in the Hydraulics Laboratory, U. S. Army Engineer Waterways Experiment Station (WES), Vicksburg, Mississippi, as a portion of the Navigation Hydraulics Program being conducted for the Office, Chief of Engineers, U. S. Army. The experimental work was completed at the National Bureau of Standards.

This report was prepared under the direction of Mr. H. B. Simmons, Chief of the Hydraulics Laboratory, by Dr. G. H. Keulegan, Special Assistant to the Chief, Hydraulics Laboratory.

Commanders and Directors of WES during the preparation and publication of this report were COL Nelson P. Conover, CE, and COL Tilford C. Creel, CE. Technical Director was Mr. F. R. Brown.

CONTENTS

SIGNIFICANT STRESSES OF ARRESTED SALINE WEDGES

PART I: INTRODUCTION

1. In 1946, an experimental program on the model laws of density currents was initiated at the National Bureau of Standards for the U. S. Army Engineer Waterways Experiment Station. The experimental work continued until 1961. Results of various studies have been reported with the exception of two studies--one relating to the interfacial stresses of the arrested saline wedges and the other, the effect of the Richardson's number on mixing. The present paper takes up the question of stresses.

2. Laboratory studies are needed on stresses of arrested saline wedges to provide guidance in the interpretation of physical models for the motion of saline waters into water courses free of large tidal influences. Constructing the model on the Froudian scale, it is necessary that the relative densities be retained. In small models the associated interfacial stresses are laminar in origin and are dependent on Reynolds number of flow (Keulegan 1955b). Since in all probability the corresponding stresses in nature would be turbulent in character, transference from the model to the prototype must be made with caution.

3. The present study reexamines further the results discussed in the report cited. Additional information is provided regarding the distribution of velocity in a cross section of the two layers, fresh and saline waters. Here, as in the previous report, attention is focused on the mean values of the stresses at the interface and at the bottom of the wedge. Flow equations are depth-integrated in both layers, the fresh water and the saline wedge. Next, resulting equations are integrated lengthwise, thereby yielding expressions for the mean stresses. Here, the derivations are repeated with more detail for clarity. Further, to examine the validity of the results involving the average stresses, the principle of momentum is applied separately once to the entire volume of fresh water lying over the wedge and next to the volume of saline water in the wedge.

PART II: APPARATUS AND PROCEDURES

4. The apparatus consists of a river forebay, a sea, and a channel connecting the two. The horizontal channel, 400 ft* long, 2 ft high, and 9 in. wide, is rectangular in cross section. The bottom consists of planed and painted wood. The sides are of glass or lucite plates, inserted into rectangular steel frames which in turn with the wooden bottom between them are attached to a steel base. The frames are 4 ft long and 2 ft high and the entire channel assembly rests on 4-ft-high concrete columns.

5. Over the forebay a metering tank is mounted to control the discharge into the channel representing the river. The bottom of the tank consists of a 1/8-in.-thick brass plate provided with numerous circular orifices of different sizes. Discharge into the channel is controlled by a chosen combination of orifices, their size and number, and the water-surface elevation in the tank. The orifices are calibrated in place by measuring the volume of water collected in the channel during a known time period with the sea end of the channel closed. The forebay is square in shape, each side is 4 ft long, and the bottom is aligned with the river channel bottom. The entrance into channel is rounded.

6. The sea is the most critical part of the entire apparatus. The 10-ft-long, 8-ft-wide, and 2-ft-deep rectangular tank representing the sea is elevated with its horizontal bottom aligned with the channel bottom. Despite the limited dimensions, the sea is required to behave as an unbounded sea. It is necessary to resort to a separate saline water reservoir placed directly below to establish a steady exchange of saline water. Return of saline water from the sea is governed by elevated crests of considerable length which also maintain a selected sea water-surface elevation. During a test run there is considerable mixing between fresh and saline waters at the sea surface and to maintain a

---

* Multiply feet by 0.3048 to convert to metres; multiply inches by 25.4 to convert to millimetres.

constant salinity of the sea, saline water from the reservoir below is constantly introduced into the sea. Previous observations have indicated that if $\rho + \Delta\rho$ be the density of seawater and $\rho + \Delta\rho'$ the density of fresh water at the locale of efflux from the sea area, as the result of mixing, the ratio $\Delta\rho'/\Delta\rho$ equals 0.34 (Keulegan 1957b). This surprisingly high value of mixing requires that the density of the saline water in the reservoir be maintained at a constant value through the continued addition of salt (Figure 1).

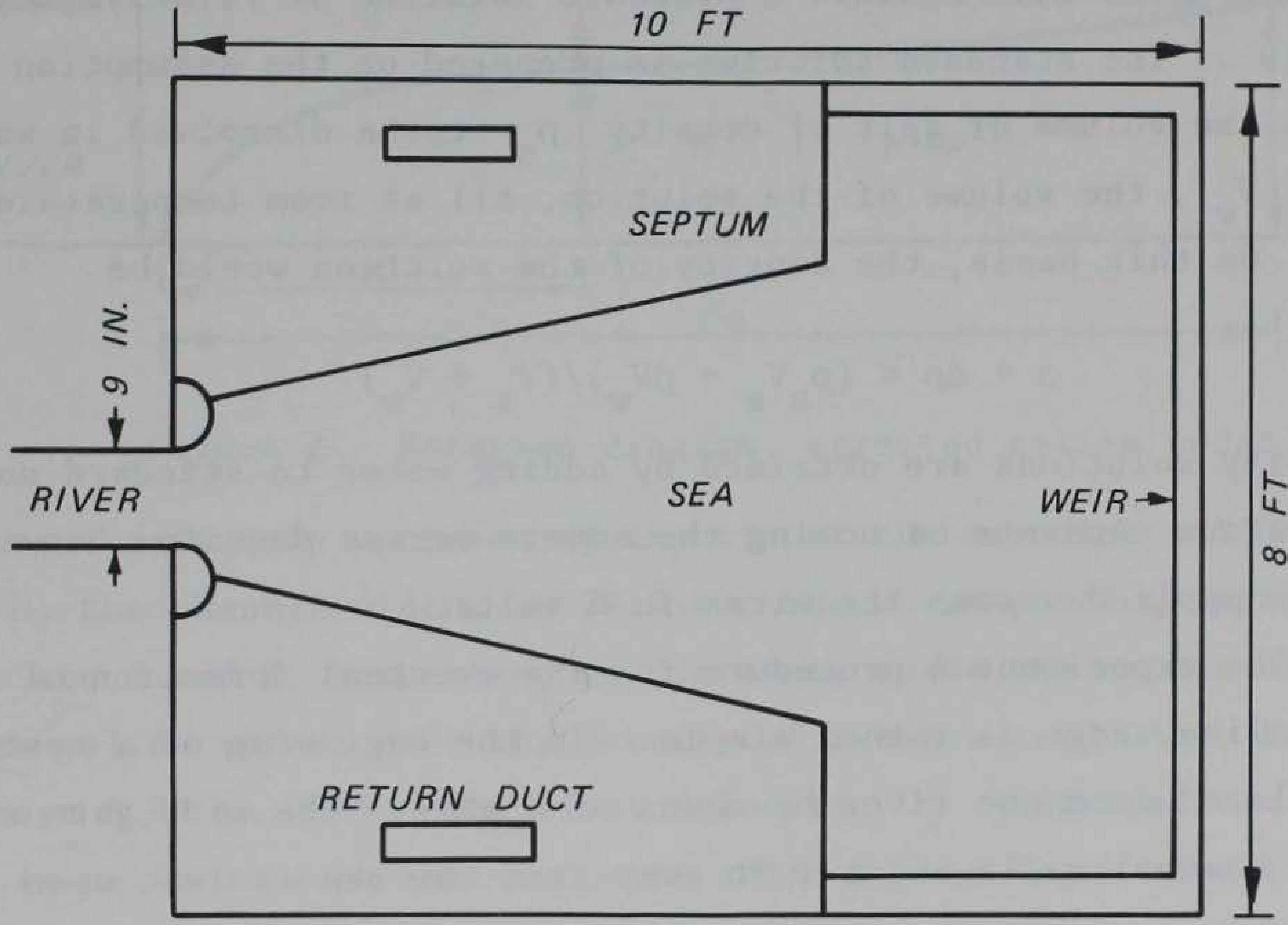

Figure 1. Plane view of experimental sea

7. Saline water densities are determined electrically by a probe, the exploring end consisting of two parallel copper or platinum wires 2 cm in length. The salinity of an electrolyte is related indirectly to the resistance between the two parallel wires immersed in a solution. If the ratio of the diameter of the wires to the spacing between them is small, the resistance is given by (Keulegan 1949):

$$R = \frac{\tau}{\pi L} \log_e \left[\frac{2s}{d}\left(1 - \frac{d^2}{4s^2}\right)\right] \tag{1}$$

where

R = effective resistance, ohms

τ = specific resistance of the electrolyte, ohms-cm

L = length of the individual wires, cm

s = spacing between wires, cm

d = diameter of the wires, cm

Since the relation applies accurately only for wires of great length, it is used for the purpose of designing the probe and selecting the ammeter. The probe is calibrated against a standard solution of relative density $\Delta\rho/\rho = 0.10$. The standard solution is prepared on the assumption that if V_s is the volume of salt of density ρ_s to be dissolved in water of volume V_w , the volume of the solution, all at room temperature, is $V_w + V_s$. On this basis, the density of the solution would be

$$\rho + \Delta\rho = (\rho_s V_s + \rho V_w)/(V_s + V_w) \tag{2}$$

Lower density solutions are obtained by adding water to standard solution. The calibration consists of noting the ampere versus density when the a-c voltage applied across the wires in 6 volts.

8. The experimental procedure for the eventual formation of an arrested saline wedge is rather simple. In the beginning of a test the sea is isolated from the river by means of a gate. The side gate at one of the channel walls about 1 ft away from the sea is left open to permit the lateral efflux of the river water. The gate is manipulated to establish the desired depth of water for the channel. With this selection, the waters in the channel and the saline water of the sea are at the same level. With this condition realized, the side gate is pushed down and the sea gate is pulled up simultaneously. This allows the entering of the river current into the sea area.

9. In the initial stages of the movement the velocity of the advancing saline front is large. With distance, the velocity decreases gradually. In the initial stages the front is rounded and also elevated. At some critical distance, the roundness of the front disappears and the front assumes the appearance of a slowly moving wedge. This form of the wedge is maintained even after the saline wave is arrested.

PART III: BASIC DATA OF THE EXPERIMENTS

10. Experiments were restricted to two river depths, $H_o = 45.5$ cm and $H_o = 23.0$ cm (Figure 2); these are the depths

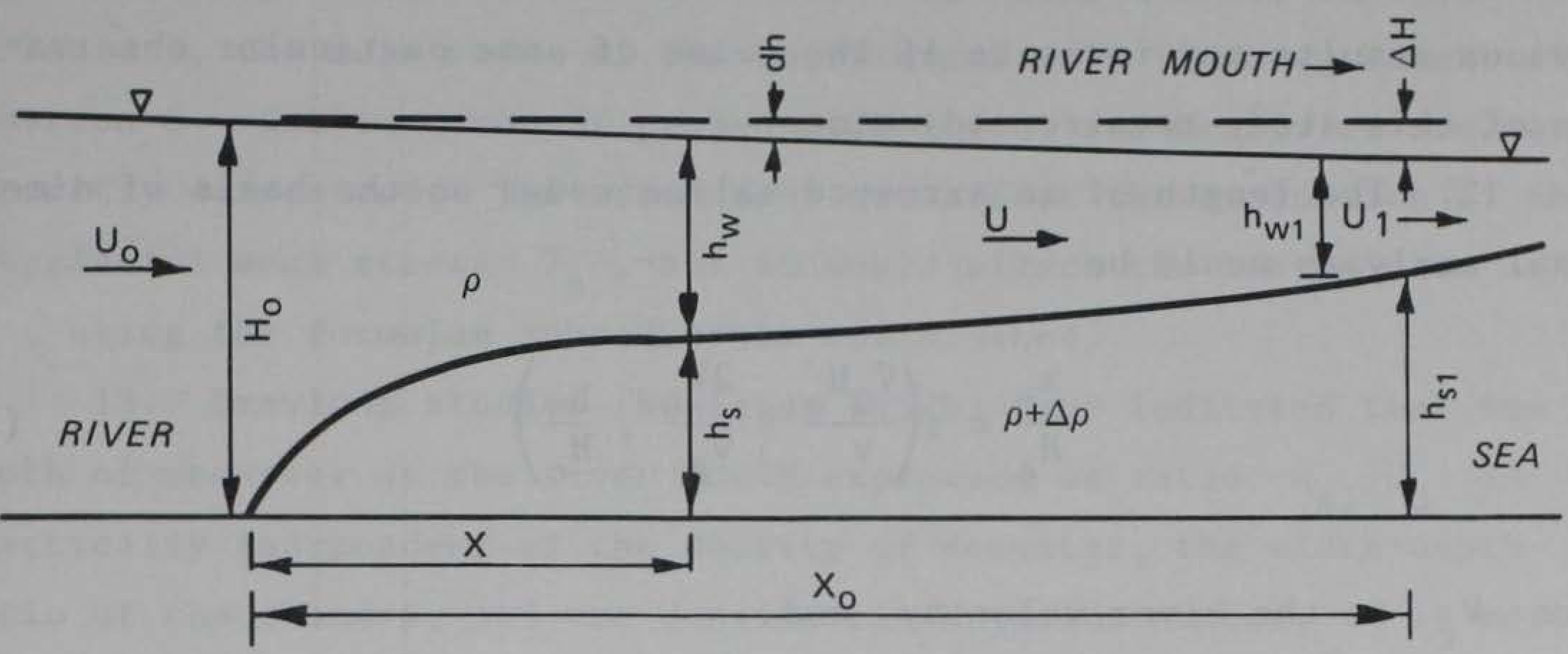

Figure 2. Notation diagram, arrested saline wedge

of water immediately upstream of the tip of the arrested saline wedge. Since B, the channel width, is 22.9 cm, the corresponding depth-width waters are 2 and 1, respectively. In these tests the excess density of the sea saline waters over the density of fresh water, $\Delta\rho$, falls in the range 0.01 to 0.08. The river velocity U_o just upstream of the wedge is selected such that n , the ratio of the depth of saline waters of wedge at the river mouth h_{s1} to water depth H_o , is close to 1/2. The data of observations regarding the river velocity U_o , the density difference $\Delta\rho$, the length of arrested saline wedge x_o , the depth of saline waters at the river mouth h_{s1} , the fall of surface waters at the river mouth ΔH , and water temperature Θ are shown in Tables 1 and 2 for the two test series. Determination of the average interfacial stress T_s , stress averaged along the entire length of the interface, and the average bottom stress T_o will be evaluated on the basis of the entries shown in these two tables. The values of $\Delta\rho$ in Table 1 are 10 percent smaller than the original measurements and the values of h_{s1} shown are 1-1/2 cm less than the original observations. The reason for these adjustments will be given subsequently.

PART IV: LENGTH OF ARRESTED SALINE WEDGES

11. Expressions for the length of the arrested saline wedges and the depth of saline waters at the river mouth in laboratory channels were established previously (Keulegan 1957b). Thus, a comparison with these previous results may indicate if the value of some particular observation of this study requires adjustment.

12. The length of an arrested saline wedge on the basis of dimensional analysis would be

$$\frac{x_o}{H_o} = f\left(\frac{V_\Delta H_o}{\nu} , \frac{2V_r}{V_\Delta} , \frac{B}{H_o}\right) \tag{3}$$

where V_r is the river velocity and

$$V_\Delta = \sqrt{\frac{\Delta\rho}{\rho} gH_o} \tag{4}$$

The ratio V_r/V_Δ is referred to as the densimetric Froude number and $V_\Delta H_o/\nu$, as the densimetric Reynolds number. When B/H_o equals unity, the wedge length is

$$\frac{x_o}{H_o} = 0.19 \left(\frac{V_\Delta H_o}{\nu}\right)^{1/2}\left(\frac{2V_r}{V_\Delta}\right)^{-5/2} , \frac{B}{H_o} = 1 \tag{5}$$

in the densimetric Reynolds number of range 1×10^4 to 10.0×10^4. In the present study the determination of length for the case $H_o = 23.0$ cm and $B = 22.9$ cm on the basis of values shown in Table 2 shows agreement with the above as the mean value of the coefficient is also 0.19. When B/H_o equals 2 in the densimetric Reynolds number of range 4.0×10^4 to 40.0×10^4 the length is given

$$\frac{x_o}{H_o} = 0.12 \left(\frac{V_\Delta H_o}{n}\right)^{1/2}\left(\frac{2V_r}{V_\Delta}\right)^{-5/2} , \frac{B}{H_o} = 1 \tag{6}$$

When the determinations of length for the case $H_o = 45.5$ cm and $B = 22.9$ cm were made on the basis of the recorded values of $\Delta\rho/\rho$, which were 10 percent higher than those shown in Table 1, the results were not in agreement with Equation 6; the mean value of the coefficient was 0.10. Repeating the determination with $\Delta\rho/\rho$ values as shown in Table 1, the mean value of the coefficient is 0.12 in agreement with Equation 6. Due to error of probe calibration, sea densities are not correctly determined. The error does not affect the evaluation of the interfacial mean stress T_s, but it would affect the bottom mean stress T_o, using the formulae subsequently established.

13. Previous studies (Keulegan 1957b) have indicated that the depth of seawater at the river mouth expressed as ratio h_{s1}/H_o is practically independent of the density of seawater, the width-depth ratio of the channel, and the densimetric Reynolds number; it is merely a function of the densimetric Froude number V_r/V_Δ as shown in Table 3. The entries represent averages from tests with different channels and different width-depth ratios (Keulegan 1957b).

14. As first shown by Shijf and Schoenfeld (1953), the flow of fresh water at the river mouth is critical,

$$\frac{U_1^2}{\frac{\Delta\rho}{\rho} gh_{w1}} = 1 \tag{7}$$

where h_{w1} is the depth of fresh water at the river mouth and U_1 is the velocity of freshwater current (Keulegan 1955a). Assuming that the fall of surface water, ΔH, is negligible one has $h_{w1} = H_o - h_{s1}$ and thus

$$\frac{h_{s1}}{H_o} = 1 - \left(\frac{V_r}{V_\Delta}\right)^{2/3} \tag{8}$$

The entries in Table 3 are in good agreement with this expression for V_r/V_Δ close to 0.5 only. For smaller values of V_r/V_Δ, theory yields depth values greater than those given in this table.

15. In the derivation of the theoretical expression, the theory assumes tacitly that the distribution of pressure is hydrostatic. On the other hand, when the densimetric Froude number is small the interface in the area of river mouth would be curved, a condition wherein the pressure would be no longer hydrostatic. Thus, it is desirable to obtain the depth h_{s1} from a relation based on observation.

16. In this study the position of the interface was obtained visually. To enhance a stronger contrast between the fresh and saline waters, the water of the sea was colored by introducing a chrome compound. This is ideal if there is no mixing at the interface. Unfortunately, if agitation is present small traces of this material may affect a deep coloring and the true position of the interface may not be inferred correctly. This was the case with the tests carried with water depth $H_o = 45.5$ cm and thus the inferred values of h_{s1} are not reliable. Indeed, the ratio H_{s1}/H when computed from the inferred values are at variance with the entries of Table 3. However, agreement would be obtained only after subtracting 1.5 cm from the inferred h_{s1}. These adjusted values of h_{s1} are shown in Table 1. A similar adjustment is not necessary for the tests carried out with water depth $H_o = 23.0$ cm.

PART V: SHAPE OF WEDGES AND FALL OF SURFACE WATERS

17. Information on the shape of the arrested saline wedge and the fall of surface waters over the wedge plays an important part in determining the average boundary stress at the interface and at the bottom from formulae.

18. Previous studies have shown that within a definite range of densimetric Froude number the shapes are affine to each other irrespective of river velocities, the density of seawater, and channel width (Keulegan 1957b). Denoting by h_s the depth of saline waters in the wedge at a point of distance x from the tip of the wedge

$$\frac{h_s}{h_{s1}} = f\left(\frac{x}{x_o}\right) \tag{9}$$

where x_o denotes the length of the wedge.
Introducing the relative distance

$$\zeta = \frac{x}{x_o} \tag{10}$$

the affine shape is

$$\frac{h}{h_{s1}} = f(\zeta) \tag{11}$$

This functional relation is shown in Table 4.

19. For the present study the observation of shape of arrested saline wedge, selecting the river water depth of ratio of $H_o = 23$ cm, is restricted to tests with a common densimetric Froude number $V_r/V_\Delta = 0.40$ and five different seawater densities. Tests with a given seawater density are repeated and the averages of h_s/h_{s1} are sought; these are shown in Table 5. Comparison between the entries of different columns indicates that for a constant densimetric Froude number the affine shape is independent of the river velocity or the

density of the seawater. The mean values from the columns are shown in the last column and these differ but little from the entries of Table 5, which apply to arrested saline wedges of varying densimetric Froude number previously studied (Keulegan 1957b). The affine depth data from Tables 4 and 5 are shown in Figure 3. The curve drawn through the points yields the relation

$$\frac{h_s}{h_{s1}} = \zeta + a \sin 2\pi\zeta \ , \quad a = 0.09 \qquad (12)$$

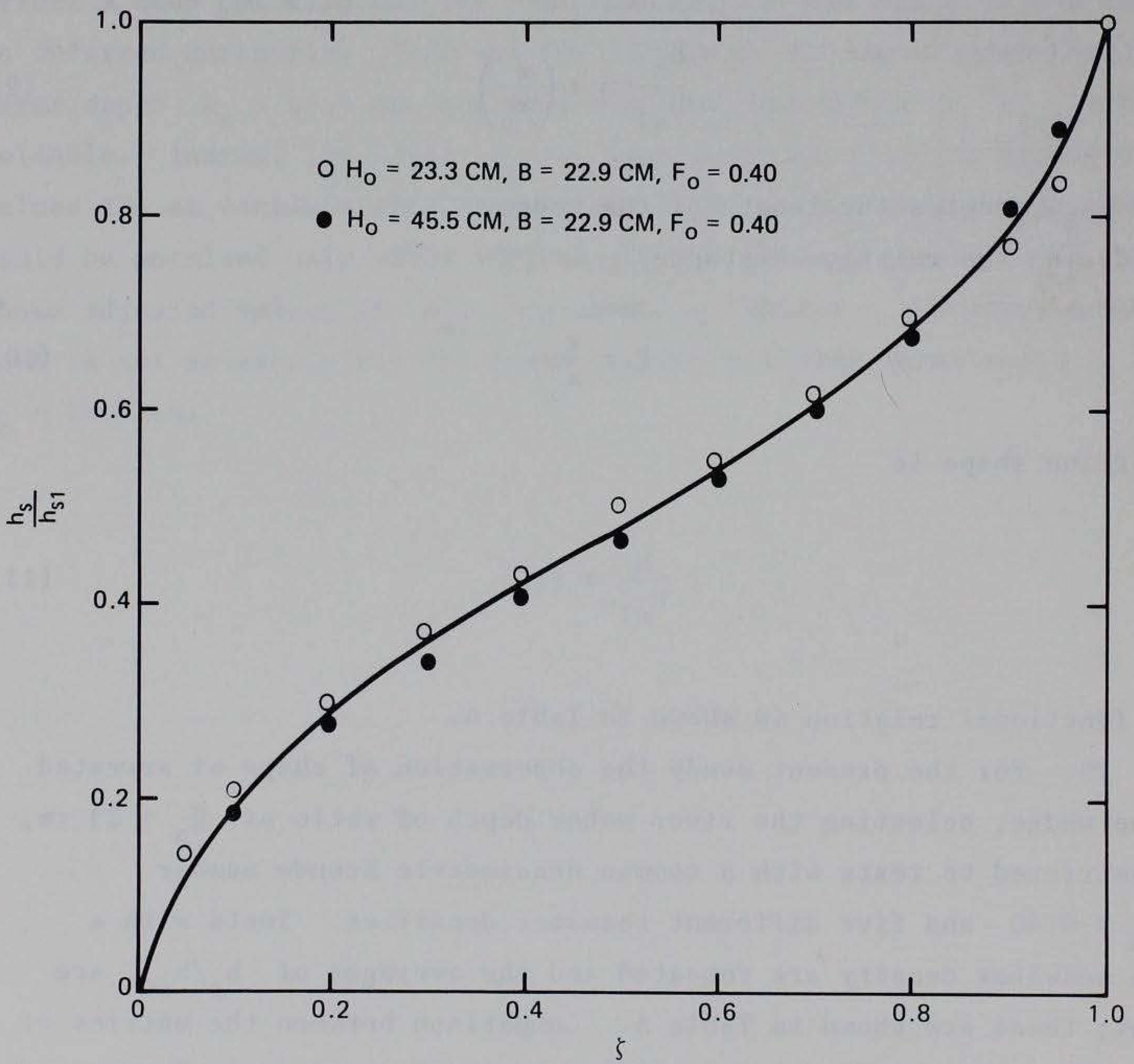

Figure 3. Affine shape of arrested saline wedge

20. To measure the fall of surface waters, along the 60-m length of the experimental channel, 12 glass manometer tubes were mounted vertically against the glass sidewalls. Next to the tubes, paper scales, (reading in centimetres) were glued to the glass. The meniscus positions were read by a telescope. Displacement of the menisci was readily estimated within a tenth of a millimetre. To establish a common zero for the scales, the exit gates of the channel were closed and the channel was filled with fresh water to a designed depth H_o, 23.0 cm or 45.5 cm. The readings of the menisci in all the manometer tubes were taken after all the surface oscillations had ceased. An example of the measurement of the fall of the freshwater free surface is given in Figure 4. The

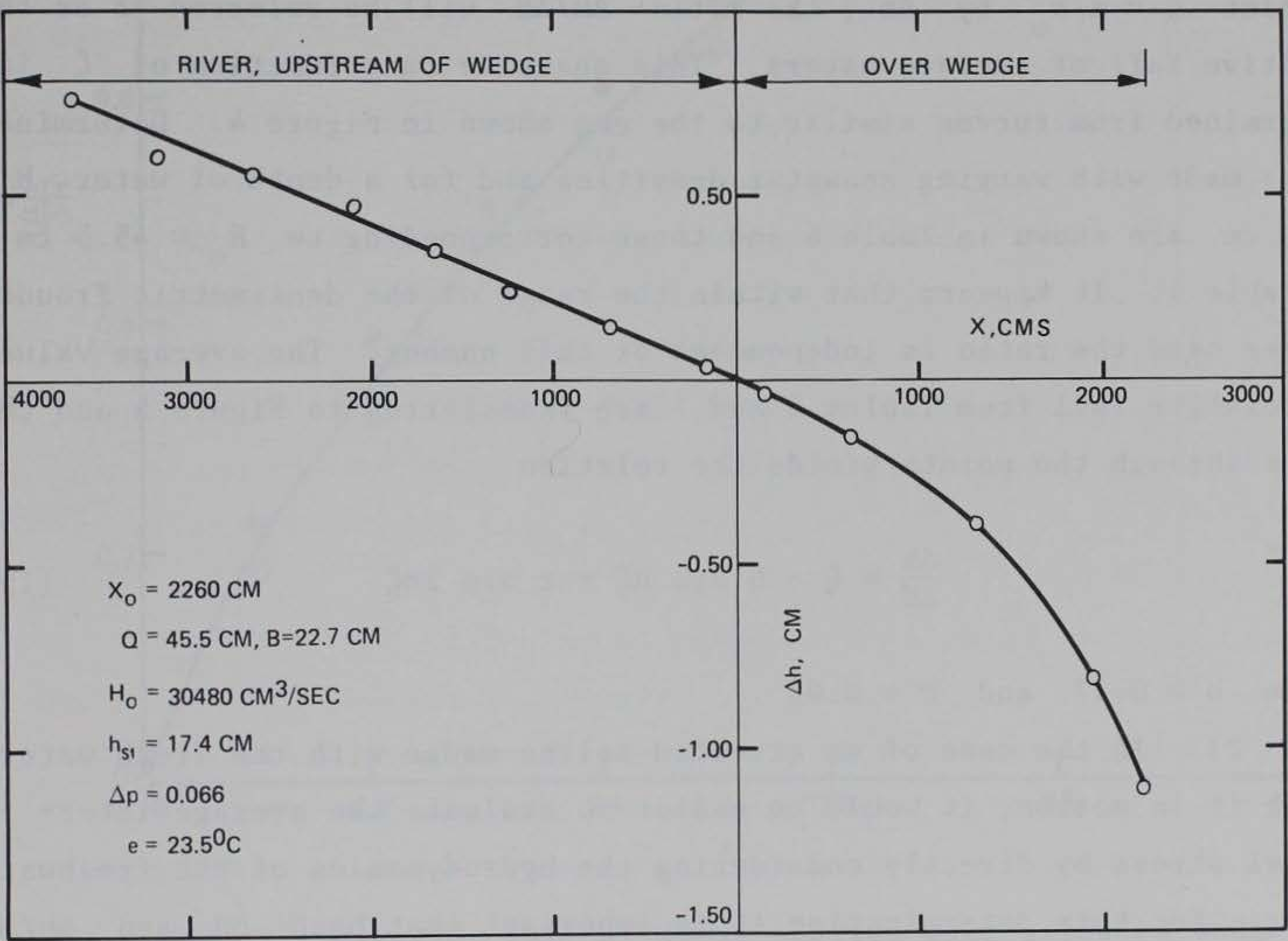

Figure 4. An example of observed values of fall of water surface

part of the curve corresponding to x negative represents the fall upstream of the tip of the arrested wedge. The slope here is in accord with the relation

$$\frac{\Delta h}{\Delta x} = -\lambda \frac{U_o^2}{2gR_h} \tag{13}$$

where R_h is the hydraulic radius and λ the coefficient of resistance

$$\lambda = 0.0559 \left(\frac{U_o R_h}{\nu}\right)^{-1/4} \tag{14}$$

The part of the curve corresponding to x positive represents the surface fall of fresh water lying over the arrested saline wedge. Denoting the fall of this surface at the river mouth by ΔH and that at a point $\zeta = x/x_o$ by Δh, the ratio $\Delta h/\Delta H$ will be referred to as the relative fall of surface waters. This quantity as a function of ζ is determined from curves similar to the one shown in Figure 4. Determinations made with varying seawater densities and for a depth of water H_o = 23.0 cm are shown in Table 6 and those corresponding to H_o = 45.5 cm in Table 7. It appears that within the range of the densimetric Froude number used the ratio is independent of this number. The average values of relative fall from Tables 6 and 7 are transferred to Figure 5 and the curve through the points yields the relation

$$\frac{\Delta h}{\Delta H} = \zeta - b \sin \pi\zeta + c \sin 2\pi\zeta \tag{15}$$

where $b = 0.17$ and $c = 0.03$.

21. In the case of an arrested saline wedge with the fresh water above it in motion, it would be easier to evaluate the average interfacial stress by directly considering the hydrodynamics of the freshwater layer. For this determination it is important that both ΔH and $\Delta h/\Delta H$ are correctly observed and evaluated.

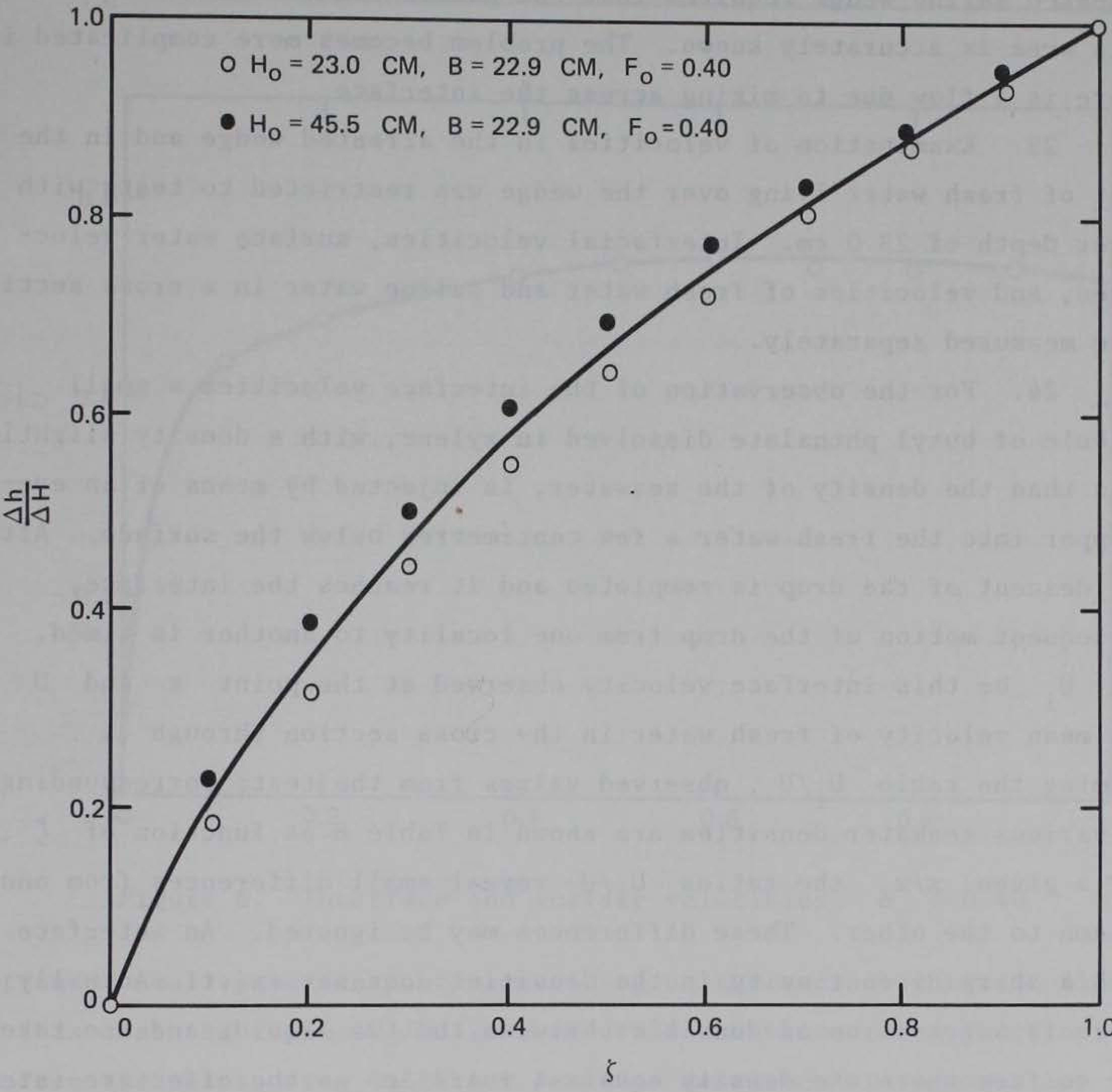

Figure 5. Relative fall of water surface over arrested wedge

PART VI: VELOCITY PATTERNS

22. The determination of the mean stress T_s of the interface and the mean bottom stress T_o on the basis of the dynamics of the arrested saline wedge requires that the pattern of the velocities in this area is accurately known. The problem becomes more complicated if there is a flow due to mixing across the interface.

23. Examination of velocities in the arrested wedge and in the part of fresh water lying over the wedge was restricted to tests with a river depth of 23.0 cm. Interfacial velocities, surface water velocities, and velocities of fresh water and saline water in a cross section were measured separately.

24. For the observation of the interface velocities a small globule of butyl phthalate dissolved in xylene, with a density slightly less than the density of the seawater, is injected by means of an eyedropper into the fresh water a few centimetres below the surface. After the descent of the drop is completed and it reaches the interface, subsequent motion of the drop from one locality to another is timed. Let U_i be this interface velocity observed at the point x and U be the mean velocity of fresh water in the cross section through x. Forming the ratio U_i/U, observed values from the tests corresponding to various seawater densities are shown in Table 8 as function of ζ. For a given x/x_o the ratios U_i/U reveal small differences from one column to the other. These differences may be ignored. An interface with a sharp discontinuity in the densities does not exist. Actually, there is a gradation of densities between the two liquids and one takes the surface where the density equals $1 + 1/2\ \Delta\rho$ as the effective interface. The density of the butyl phthalate globules cannot be accurately controlled and in different tests the globules are differently placed with respect to the interface. It is thus sufficient to consider the average values entered in the last column of Table 8. The plotting in Figure 6 is on this basis. Starting from zero, the value of U_i/U increases very rapidly and then slowly reaches asymptotically the limit $U_i/U = 0.53$. The surface velocity U_s is determined by timing the

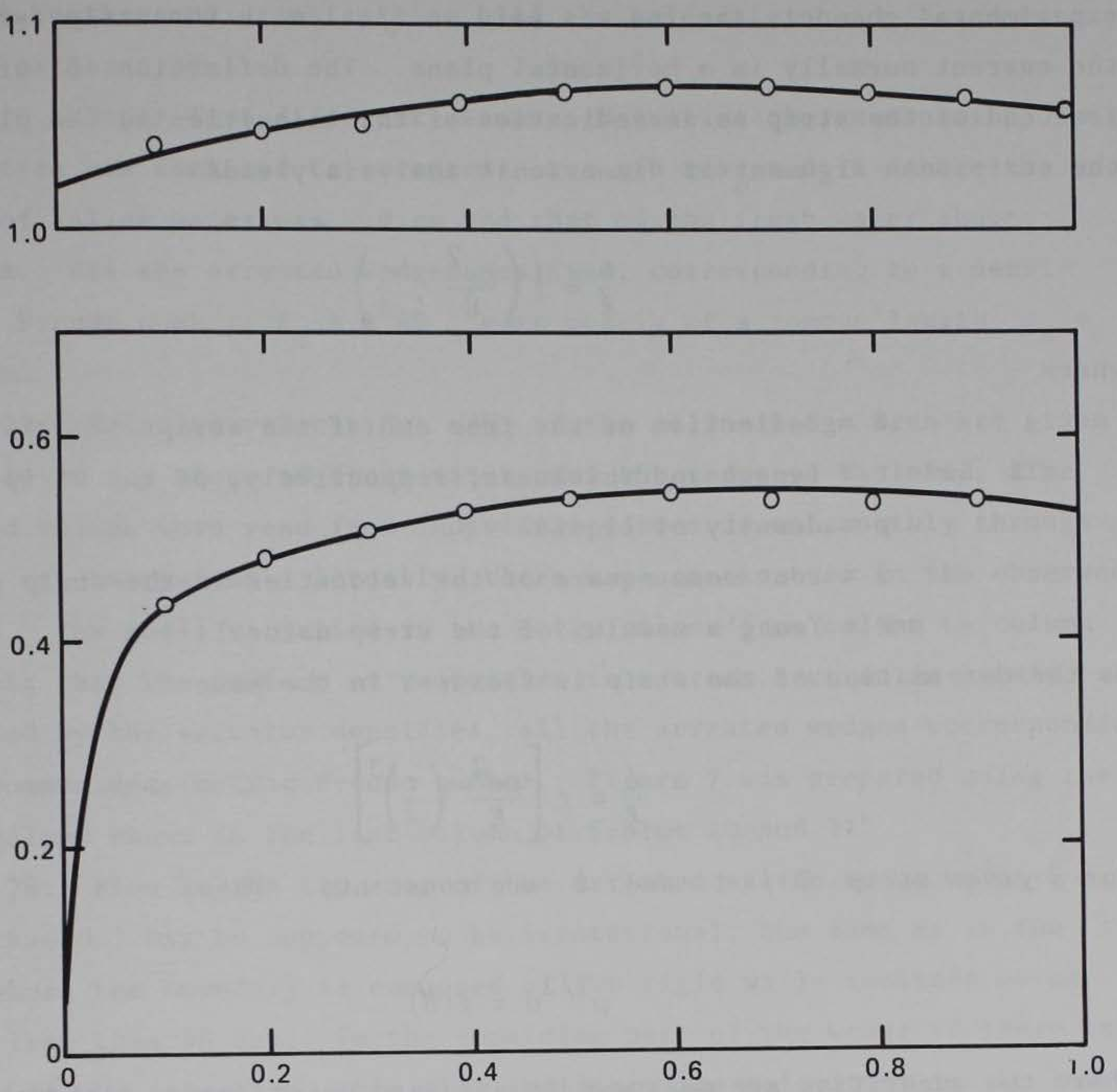

Figure 6. Interface and surface velocities, $F_o = 0.40$

motion of small paraffin particles riding on the surface waters. Also, in this case the ratio U_s/U is formed and the values as a function of ζ from the tests using different seawater densities are entered in Table 9. Here also U_s/U values reveal small differences from one column to the other. The average values are entered in the last column and the plotting in Figure 6 is on this basis.

25. The device to determine the distribution of the velocities in a flow cross section consisted of a thin phosphor bronze strip about 1/4 in. wide and 8-1/2 in. long with one of the ends of the strip soldered to a rectangular rod. Touching one of the sidewalls of the

experimental channel, the rod was held vertical with the strip facing the current normally in a horizontal plane. The deflection δ of the free end of the strip is an indication of the velocities in the plane of the strip. An argument of dimensional analysis yields

$$\frac{\delta}{\ell} = f\left(\frac{\rho u^2}{E}, \frac{t}{\ell}\right) \tag{16}$$

where

δ = deflection of the free end of the strip

ℓ and t = length and thickness, respectively, of the strip

ρ = density of liquid

u = root mean square of the velocities in the strip plane

E = Young's modulus of the strip natural

As the deformation of the strip is flexural in the main

$$\frac{\delta}{\ell} = f\left[\frac{\rho u^2}{E}\left(\frac{t}{\ell}\right)^3\right] \tag{17}$$

For a given strip E, t and ℓ are constants. Then,

$$\rho^{1/2}u = f(\delta) \tag{18}$$

where the quantities are measured in standard units, cgs. Although the relation may be established using Kirchhoff's theory of slender wires, it is more practical to resort to calibration. For this purpose the strip is held at middepth of a current in the experimental channel of discharge Q and the end deflection δ is noted. The average velocity u is deduced from the discharge and the strip elevation from the channel bottom using Blasius' velocity relation. It is assumed that the velocities of all the points in a cross section having the same common elevation are equal. This introduces a small calibration error since the velocities at the points of strip level are not constant. This, however, will not severely affect the value of u/U, where u is the root-mean-square value of the velocities at points of a common elevation from the bottom and U is the average velocity of the freshwater current in the same cross section, all the velocities being based on a chosen calibration.

26. Using five different seawater densities the examination of velocities was confined to a central area of $x/x_o = 0.75$ where the depth of saline water was 7.0 cm and that of the fresh water above, 16.0 cm. All the arrested wedges realized, corresponding to a densimetric Froude number $F_o = 0.40$, were nearly of a common length x_o = 2000 cm.

27. Relative velocities u/U of the saline wedge area are given in Table 10 and those of fresh water over the wedge in Table 11. The entered values were read from individual curves drawn smoothly through points of observation. Actually, there was some scatter in the observed values. The small variation in the entry values from column to column suggests that the pattern of velocities in a cross section is hardly affected by the seawater densities, all the arrested wedges corresponding to a common densimetric Froude number. Figure 7 was prepared using the mean values shown in the last column of Tables 10 and 11.

28. Flow in the tip area of the arrested saline wedge with ζ less than 0.1 may be supposed to be irrotational, the same as in the case where the boundary is composed of two rigid walls inclined at an angle less than 90 deg. In the remaining part of the wedge if there is mixing at the interface, this will influence the velocities in the lower areas of the arrested wedge where the motion is away from the sea. Using the methods of an earlier investigation on mixing in arrested saline wedges (Beta 1957), it may be estimated that the total quantity of saline water traversing the interface into fresh water due to mixing is about 8 percent of the saline water inflow into the wedge from the sea. The effect of this may be ignored. One may then assume that the velocity patterns from one cross section to another are similar to each other. It was already seen that the interfacial velocity U_i/U has practically the same value along almost the entire length of the interface except in the area near the tip.

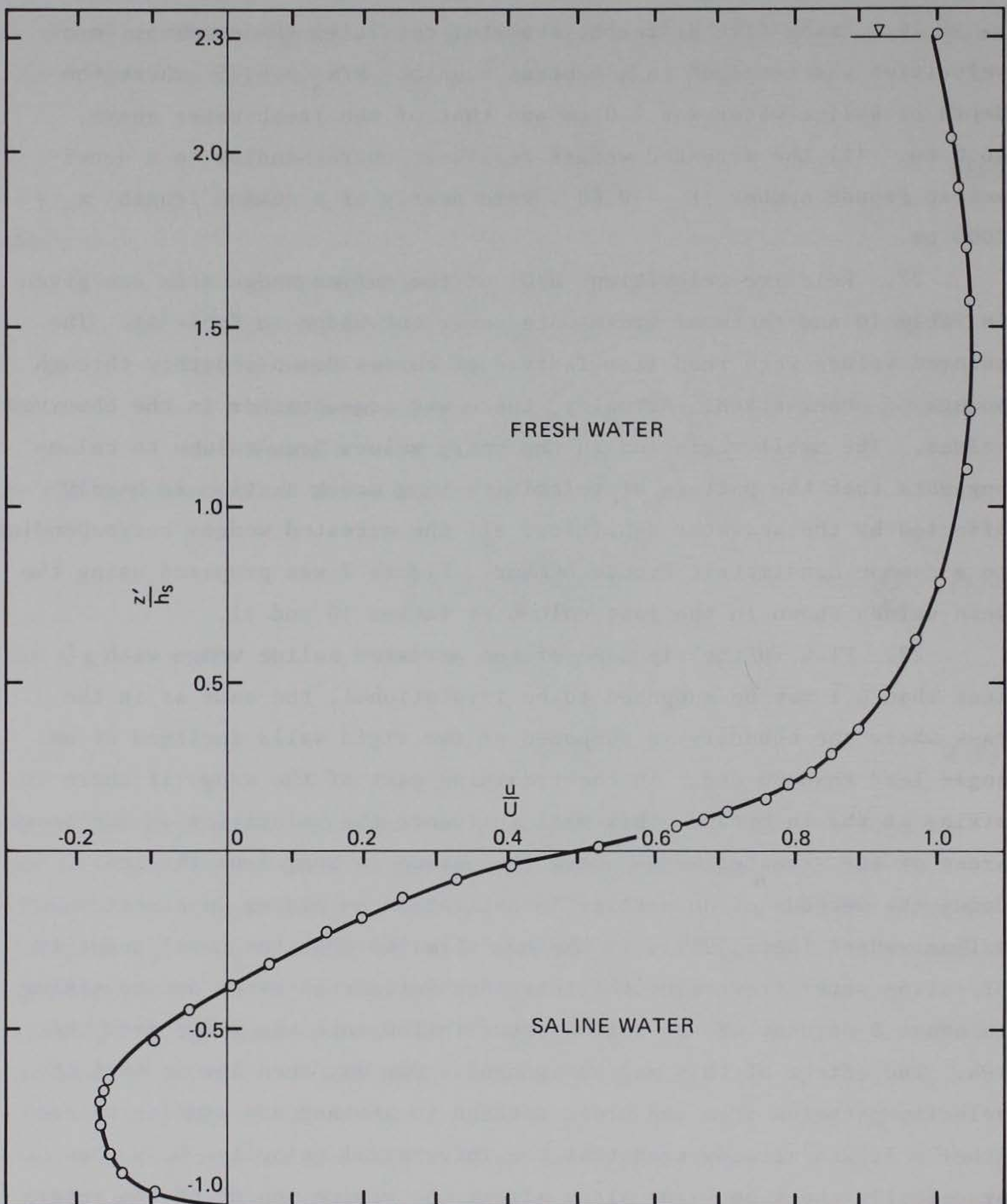

Figure 7. Fresh and saline water velocities in arrested saline wedges, $F_o = 0.40$

29. Let the origin of the rectangular axis system be placed at the tip of the arrested saline wedge and at the midpoint of the channel bottom width. Let the axis of x be drawn horizontally in the direction of motion of the fresh water and z vertically upward. Components of the velocities along the axes x, y, and z are u, v, and w, respectively. Elevation of the water surface measured from the horizontal channel bottom may be denoted by h and that of the interface by h_s. Let the width of the channel be B, $B = 2b$ (Figure 8).

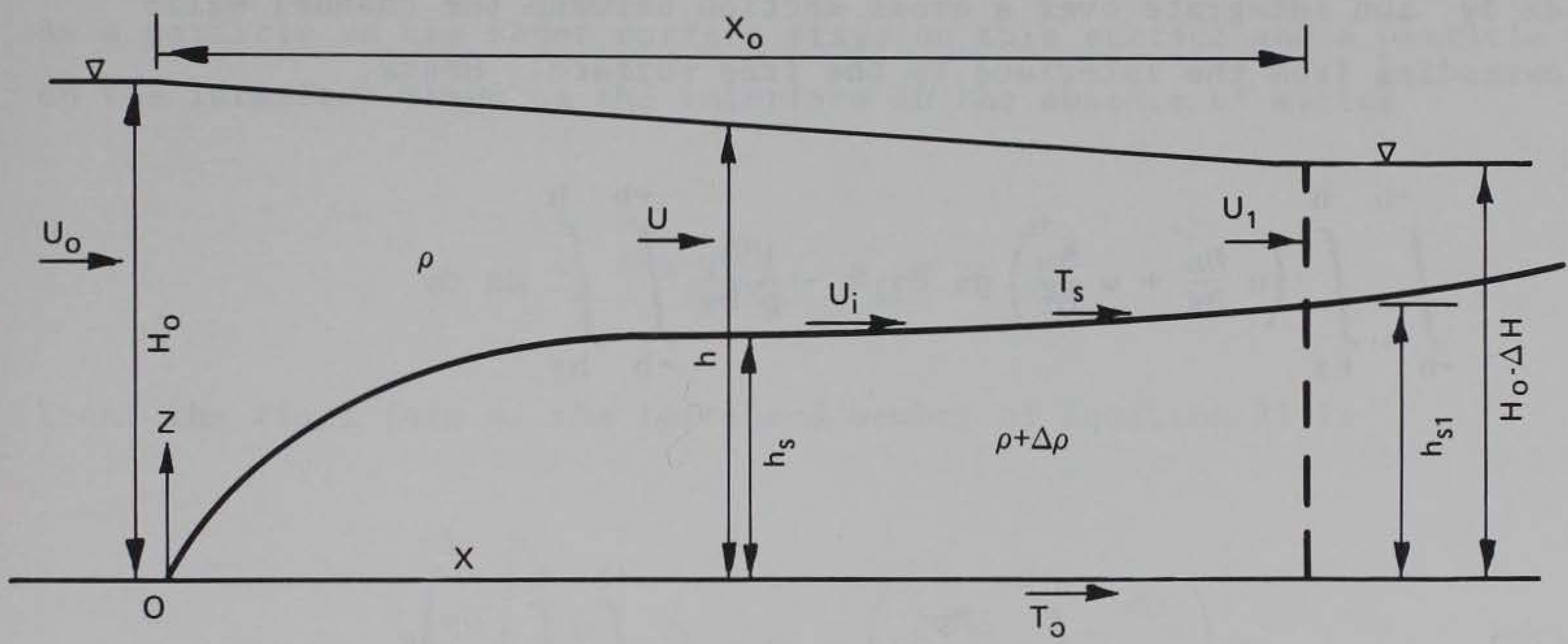

Figure 8. Notation diagram, analysis of wedge stresses

30. As the length of the arrested saline wedge is large in comparison with the maximum depth h_{s1} of the wedge at the river mouth, the vertical component of the fluid acceleration will be neglected and the pressure will be evaluated hydrostatically. Under this assumption, using the notation of Lamb, the equations of motion are

$$u \frac{\partial u}{\partial x} + w \frac{\partial u}{\partial z} = - \frac{1}{\rho} \frac{\partial p}{\partial x} + \frac{1}{\rho} \left(\frac{\partial p_{zx}}{\partial z} + \frac{\partial p_{yx}}{\partial y} \right) \qquad (19)$$

and

$$0 = -\frac{1}{\rho}\frac{\partial p}{\partial z} - g \tag{20}$$

Here p_{zx} denotes the tangential stress which the liquid of increasing z exerts on a plane surface normal to z axis and in the direction of x. Similarly p_{yx} is the tangential stress which the liquid of the increasing y exerts on a plane surface normal to y axis and in the direction of x. Again, ρ is the density of water, p is the pressure, and g is the gravitational contact.

31. The hydrodynamics of the freshwater flow over the arrested wedge will be considered first. Multiply the terms in Equation 19 by $dz\,dy$ and integrate over a cross section between the channel walls extending from the interface to the free surface. Hence,

$$\int_{-b}^{+b}\int_{hs}^{h}\left(u\frac{\partial u}{\partial x} + w\frac{\partial u}{\partial z}\right)dz\,dy = -\frac{1}{\rho}\frac{\partial p}{\partial x}\int_{-b}^{+b}\int_{hs}^{h} dz\,dy$$

$$+\frac{1}{\rho}\int_{-b}^{+b}\frac{\partial p_{zx}}{\partial z}\,dz\,dy + \frac{1}{\rho}\int_{-b}^{+b}\int_{h_s}^{h}\frac{\partial p_{yx}}{\partial y}\,dz\,dy\,. \tag{21}$$

Since the liquid is incompressible

$$\frac{\partial u}{\partial x} + \frac{\partial w}{\partial z} = 0$$

and one now has

$$w\frac{\partial u}{\partial z} = \frac{\partial}{\partial z}(uw) + u^2\frac{\partial u}{\partial x}$$

Substituting this in the left-hand member of Equation 19 this now becomes

$$\int_{-b}^{+b} \int_{hs}^{h} \left[\frac{\partial}{\partial x} (u^2) + \frac{\partial}{\partial z} (uw) \quad dz \ dy \right]$$

or

$$\int_{-b}^{+b} \int_{hs}^{h} \frac{\partial}{\partial x} u^2 \ dz \ dy + \left[(uw)_s - (uw)_i \right] B$$

where the subscript "s" refers to the surface and "i" to the interface. As a particle on the water surface stays on this surface and a particle on the interface stays on the interface in the absence of mixing

$$w_s = u_s \frac{dh}{dx} , \quad w_i = u_i \frac{dh_s}{dx}$$

Then, the final form of the left-hand member of Equation 21 is

$$\int_{-b}^{+b} \int_{h_s}^{h} \frac{\partial}{\partial x} u^2 \ dz \ dy + \left(u_s^2 \frac{dh}{dx} - u_i^2 \frac{dh_s}{dx} \right) B \tag{22}$$

One now introduces α , the Boussinesq coefficient of velocity distribution, defined by

$$\alpha U^2 A = \int_{-b}^{+b} \int_{h_s}^{h} u^2 \ dx \ dz \tag{23}$$

where U is the average value of u in a cross section $A = B(h - h_s)$. Differentiating the two sides of this last equation with respect to x , in accordance with the Leibnitz rule,

$$\frac{d}{dx}\,(\alpha U^2 A) = \int_{-b}^{+b} \int_{h_s}^{h} \frac{\partial}{\partial x}\, u^2 \; dz \; dy + \left(u_s^2 \, \frac{dh}{dx} - u_i^2 \, \frac{dh}{dx} \right) B$$

Hence after comparing with Equation 22, the left-hand member of Equation 21 is

$$\int_{h_s}^{h} \int_{-b}^{+b} \left(u \, \frac{\partial u}{\partial x} + w \, \frac{\partial u}{\partial z} \right) dz \; dy = \frac{d}{\partial x} \left(\alpha U^2 A \right) \tag{24}$$

A slight variation of α with respect to x may be ignored and as UA is constant

$$\frac{d}{dx}\,(\alpha U^2 A) = UA \, \frac{d}{dx}\,(\alpha U) = \frac{\alpha}{2}\, A \, \frac{dU^2}{dx} = \frac{\alpha}{2}\, \frac{dU^2}{dx}\,(h - h_s) B \tag{25}$$

Thus finally

$$\int_{-b}^{+b} \int_{h_s}^{h} \left(u \, \frac{\partial u}{\partial x} + w \, \frac{\partial u}{\partial z} \right) dz \; dy = \frac{\alpha}{2}\, \frac{dU^2}{dx}\,(h - h_s) B \tag{26}$$

This is an evaluation of the integral on the left-hand side of Equation 21. From Equation 20

$$p = p_a + \rho g(h - z) \qquad\qquad h \geq h_s$$

where p_a is the atmospheric pressure. Accordingly, the first integral on the right-hand side of Equation 21 reduces to

$$-\frac{1}{\rho}\frac{\partial p}{\partial x}\int_{-b}^{+b}\int_{h_s}^{h} dz\,dy = -g\,\frac{dh}{dx}\,(h - h_s)B \qquad (27)$$

In the absence of air currents, the stress at the water surface vanishes. Let the traction of the fresh water on the saline water be denoted by τ_s . Thus

$$p_{zx} = 0 \qquad z = h$$

$$p_{zx} = \tau_s \qquad z = h_s$$

and the second integral on the right-hand side of Equation 21 reduces to

$$\frac{1}{\rho}\int_{-b}^{+b}\int_{h_s}^{h}\frac{\partial p_{zx}}{\partial z}\,dz\,dy = -\frac{1}{\rho}\int_{-b}^{+b}\tau_s\,dy = -\frac{1}{\rho}\,\bar{\tau}_s B \qquad (28)$$

where $\bar{\tau}_s$ is the average value of the interfacial stress along the channel width. It is a positive quantity. Denoting the resistive force of the vertical wall by τ_w , a positive quantity,

$$p_{yx} = -\tau_w \qquad y = b$$

$$p_{yx} = \tau_w \qquad y = -b$$

the third integral on the right-hand side of Equation 21 reduces to

$$\frac{1}{\rho}\int_{-b}^{b}\int_{h_s}^{h} \frac{\partial p_{yx}}{\partial y}\, dz\, dy = -\frac{2}{\rho}\int_{h_s}^{h} \tau_w dz = -\frac{2}{\rho}\bar{\tau}_w (h - h_s) \qquad (29)$$

where $\bar{\tau}_w$ is the average value of the wall shear across the span $h - h_s$. In view of Equations 26, 27, 28, and 29, the original Equation 21 reduces to

$$\frac{\bar{\tau}_s}{\rho} = -g\frac{dh}{dx}(h - h_s) - 2\frac{\bar{\tau}_w}{\rho}\frac{(h - h_s)}{B} - \frac{\alpha}{2}\frac{dU^2}{dx}(h - h_s) \qquad (30)$$

This is the expression for the local stress in terms of the surface slope, the surface elevation, the saline wedge height, and the current mean velocity. All these refer to the situation at the point x. However, owing to the difficulties in measuring the surface fall rate dh/dx accurately, it will prove to be more serviceable to consider the average T_s of the interface stress, averaged along the entire length of the saline wedge.

$$T_s x_o = \int_o^{x_o} \bar{\tau}_s\, dx \qquad (31)$$

and in view of Equation 30

$$\frac{T_s}{\rho} = -g \int_o^{x_o} \frac{dh}{dx} (h - h_s) \frac{dx}{x_o}$$

$$- \frac{2}{B} \int_o^{x_o} \frac{\bar{\tau}_w}{\rho} (h - h_s) \frac{dx}{x_o} - \frac{\alpha}{2} \int_o^{x_o} \frac{dU^2}{dx} (h - h_s) \frac{dx}{x_o} \tag{32}$$

Since

$$U_o H_o = U_1 (H_o - \Delta H - h_{s1}) = U(h - h_s) \tag{33}$$

where U_1 is the velocity of fresh water at the river mouth and ΔH the fall of surface, the last term in Equation 32 changes to

$$\alpha \frac{U_1^2 (H_o - \Delta H - h_{s1}) - U_o^2 H_o}{x_o} \tag{34}$$

Also, neglecting ΔH^2

$$\frac{1}{x_o} \int_o^{x_o} h \frac{dh}{dx} dx = \frac{1}{x_o} \int_o^{x_o} hdh = - \frac{H_o \Delta H}{x_o} \tag{35}$$

and

$$\int_o^{x_o} h_s \frac{dh}{dx} \frac{dx}{x_o} = - \int_o^{x_o} h_s \frac{d\Delta h}{dx} \frac{dx}{x_o} \tag{36}$$

For brevity introduce T_{w1} the total frictional force of the walls on the fresh water

$$T_{w1} = 2 \int_{o}^{x_o} \bar{\tau}_w (h - h_s)\, dx \tag{37}$$

In view of the last four relations, Equation 32 changes to

$$\frac{T_s}{\rho} = gH_o \left(\frac{\Delta H}{x_o} - \int_{o}^{x_o} \frac{h_s}{H_o} \frac{d\Delta h}{dx} \frac{dx}{x_o} \right) - \frac{T_{w1}}{\rho B x_o} - \frac{\alpha \left[U_1^2 \left(H_o - \Delta H - h_{s1} \right) - U_o^2 H_o \right]}{x_o} \tag{38}$$

32. One may also obtain this relation by applying the principle of momentum to the body of water found at the instant t over the wedge with its boundary ABDE as shown in Figure 9. Let dM/dt denote the rate of change of momentum of this water in the direction x positive.

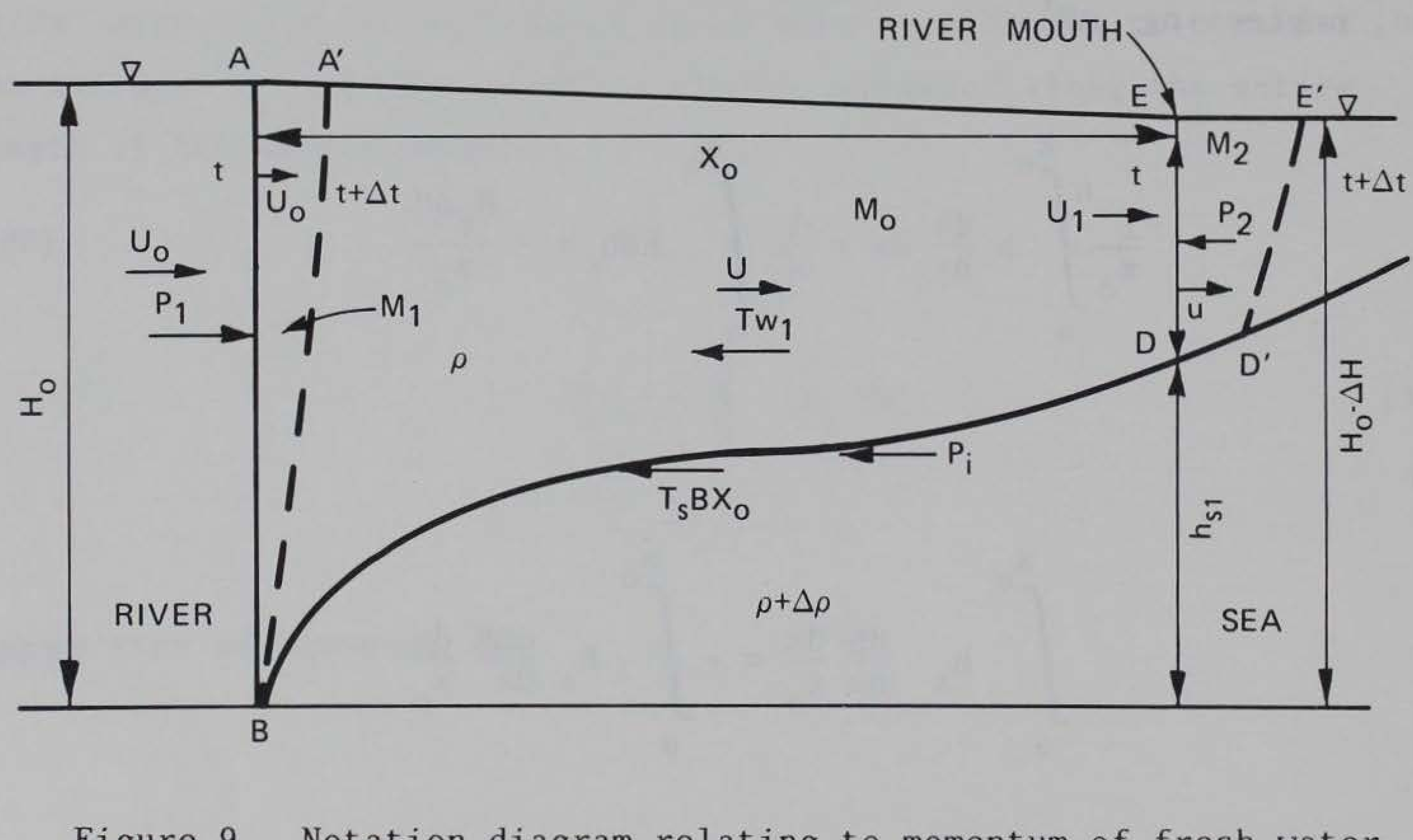

Figure 9. Notation diagram relating to momentum of fresh water

The forces producing this change are the pressure forces P_1 and P_2 acting on the upstream and the downstream forces AB and ED, and the pressure force P_i on the interface. The tangential traction forces taking part in this change of momentum are T_{w1}, the retracting force from the two sidewalls, and $T_s Bx_o$, the retracting force due to the saline wedge. Thus

$$\frac{\delta M}{\delta t} = P_1 - P_2 - P_i - T_{w1} - T_s B x_o \tag{39}$$

The particles of water which at time t are in the planes AB and DE move into the surfaces A'B and D'E' at time $t + \delta t$, respectively. Let M_o be the momentum of the liquid contained in A'BDE; M_1 of that contained in ABA'; and M_2 of that contained in EDD'E'. On this basis the momentum of liquid under consideration is $M_o + M_1$ at the instant t and $M_o + M_2$ at the instant $t + \delta t$. Thus the rate of change of momentum is

$$\frac{\partial M}{\partial t} = (M_2 - M_1)\delta t \tag{40}$$

Now,

$$M_1 = \rho \int_o^{H_o} \int_{-b}^{+b} u_o^2 \, dz \, dy \, \delta t = \alpha_1 \rho U_o^2 H_o B \delta t$$

and

$$M_2 = \rho \int_{h_{s1}}^{H_o - \Delta H} \int_{-b}^{+b} u_1^2 \, dz \, dy \, \delta t = \alpha_2 \rho U_1^2 (H_o - \Delta H - h_{s1}) \delta t$$

where U_o is the river current average velocity at the tip of the saline wedge and U_1 the average velocity of fresh water at the river mouth.

Introducing these in Equation 40 and assuming $\alpha_2 = \alpha_2 = \alpha$

$$\frac{\delta M}{\delta t} = \rho\alpha \left[U_1^2 (H_o - \Delta H - h_{s1}) - U_o^2 H_o B \right] \tag{41}$$

Ignoring the pressure of the atmosphere, the end pressure forces are

$$P_1 = \rho g \frac{H_o^2}{2} B$$

and

$$P_2 = \rho g \frac{(H_o - \Delta H - h_{s1})^2}{2} B$$

Thus, ignoring ΔH^2

$$P_1 - P_2 = \rho g B \left(H_o \Delta H + H_o h_{s1} - \Delta H h_{s1} - \frac{h_{s1}^2}{2} \right) \tag{42}$$

The total pressure force from the interface is

$$P_i = \rho g B \int_o^{h_{s1}} (H_o - \Delta h_o - h_s) \, dh_s$$

or

$$P_i = \rho g B \left(H_o h_{s1} - \frac{h_{s1}^2}{2} - \int_o^{x_o} \Delta h \frac{dh_s}{dx} dx \right)$$

Now

$$\frac{d}{dx} (\Delta h h_s) = \Delta h \frac{dh_s}{dx} + h_s \frac{d\Delta h}{dx}$$

and as

$$\int_o^{x_o} \frac{d}{dx} (\Delta h h_s)\, dx = \Delta H h_{s1}$$

finally

$$P_i = \rho g B \left(H_o h_{s1} - \frac{h_{s1}^2}{2} - \Delta H h_{s1} + \int_o^{x_o} h_s \frac{d\Delta h}{dx} dx \right) \tag{43}$$

From Equations 42 and 43

$$P_1 - P_2 - P_i = \rho g B \left(H_o \Delta H - \int_o^{x_o} h_s \frac{d\Delta h}{dx} \Delta x \right) \tag{44}$$

Substituting from Equations 41 and 44 in Equation 39 and dividing the resulting equation by $\rho B x_o$

$$\frac{T_s}{\rho} = g H_o \left(\frac{\Delta H}{x_o} - \int_o^{x_o} \frac{h_s}{H_o} \frac{d\Delta h}{dx} \frac{dx}{x_o} \right) - \frac{T_{w1}}{\rho B x_o} - \alpha \frac{\left[U_1^2 (H_o - \Delta H - h_{s1}) - U_o^2 H_o \right]}{x_o} \tag{45}$$

This last equation is identical with Equation 38, the alternate form of Equation 32 which was derived by integrating vertically the Eulerian flow, Equation 19.

PART VIII: HYDRODYNAMICS OF ARRESTED SALINE WEDGE AND AVERAGE BOTTOM STRESS

33. Multiplying the terms in Equation 19 by dz dy and integrating over the cross section of the wedge at x ,

$$\int_{-b}^{+b}\int_{o}^{h_s}\left(u\frac{\partial u}{\partial x}+w\frac{\partial u}{\partial z}\right)dz\ dy=-\frac{1}{\rho'}\int_{-b}^{+b}\int_{o}^{h_s}\frac{\partial p}{\partial x}\,dz\ dy$$

$$+\frac{1}{\rho'}\int_{-b}^{+b}\int_{o}^{h_s}\frac{p_{zx}}{\partial z}\,dz\ dy+\frac{1}{\rho'}\int_{-b}^{+b}\int_{o}^{h_s}\frac{\partial p_{yx}}{dy}\,dz\ dy \qquad (46)$$

where ρ' is the density of saline waters of the edge. Since in the normal cross section of the arrested saline wedge the mean velocity U practically vanishes, one now introduces, in establishing an expression similar to Equation 23, the interfacial velocity U_i and defines a new coefficient of velocity β as

$$\beta U_i^2 A=\int_{-b}^{+b}\int_{o}^{h_s}u^2\,dz\ dy \qquad (47)$$

Using the same argument that was applied to the freshwater part it may be shown that

$$\int_{o}^{h_s}\int_{-b}^{+b}u\left(\frac{\partial u}{\partial x}+w\frac{\partial u}{\partial z}\right)dz\ dy=B\frac{d}{dx}\left(\beta U_i^2 h_s\right) \qquad (48)$$

Assuming that the pressure is hydrostatic also in the wedge

$$p = p_a + \rho g(h - h_s) + g(\rho + \Delta\rho)(h_s - z) \ , \ z \leq h_s$$

where $\Delta\rho$ is the excess of density of the saline water of the wedge over that of fresh water; $\rho' = \rho + \Delta\rho$. Differentiating with respect to x

$$\frac{\partial p}{\partial x} = g\left(\rho \frac{\partial h}{\partial x} + \Delta\rho \frac{\partial h_s}{\partial x}\right)$$

and setting in the first integral of the right-hand side of Equation 46

$$- \int_{o}^{h_s} \int_{-b}^{+b} \frac{1}{\rho'} \frac{\partial p}{\partial x} \, dz \, dy = -g\left(\frac{\partial h}{\partial x} + \frac{\Delta\rho}{\rho} \frac{\partial h_s}{\partial x}\right) \ h_s B \qquad (49)$$

since ρ'/ρ is practically unity. Denoting the frictional stress of the bottom by τ_o

$$p_{zx} = \tau_s \qquad\qquad z = h_s$$

$$p_{zx} = -\tau_o \qquad\qquad z = 0$$

the quantities τ_s and τ_o being regarded as positive. The second integral on the right-hand side of Equation 42 now becomes, neglecting again the difference between ρ and ρ' ,

$$\frac{1}{\rho'} \int_{-b}^{+b} \int_{o}^{h_s} \frac{\partial p_{zx}}{\partial z} \, dz \, dy = \frac{1}{\rho} \int_{-b}^{+b} (\tau_s + \tau_o) \, dy = + \frac{1}{\rho}\left(\bar{\tau}_s + \bar{\tau}_o\right) B \qquad (50)$$

In regard to the sidewall effect

$$p_{yx} = -\tau_w \qquad y = b$$

$$p_{yx} = +\tau_w \qquad y = -b$$

Here τ_w is positive when the flow in the neighborhood of the wall is in the direction of the main flow of fresh water above and negative when in the opposite direction. The sign of τ_w changes from the positive to the negative in moving from the interface downward. Now,

$$\frac{1}{\rho'}\int_{-b}^{+b}\int_{o}^{h_s} \frac{\partial p_{yx}}{\partial y}\, dz\, dy = -\frac{2}{\rho}\int_{o}^{h_s} \tau_w\, dz = -\frac{2}{\rho}\,\bar{\tau}wh_s \tag{51}$$

Substituting the expression from Equations 48, 49, 50, and 51 in Equation 46, dividing by B, and transferring terms

$$\frac{\bar{\tau}_s}{\rho} + \frac{\bar{\tau}_o}{\rho} = g\left(\frac{\partial h}{\partial x} + \frac{\Delta\rho}{\rho}\,\frac{dh_s}{dx}\right) h_s + \frac{2}{\rho}\;\bar{\tau}_w\,\frac{h_s}{B} + \frac{d}{dx}\left(\beta U_i^2 h_s\right) \tag{52}$$

Multiplying the terms in this equation by dx, integrating between the limits $x = 0$ and $x = x_o$, and writing

$$T_o x_o = \int_o^{x_o} \bar{\tau}_o\, dx \tag{53}$$

$$\frac{T_s}{\rho} + \frac{T_o}{\rho} = g\int_o^{x_o} \frac{dh}{dx}\, h_s\, \frac{dx}{x_o} + \frac{1}{2}\, g\, \frac{\Delta\rho}{\rho}\, \frac{h_{s1}^2}{x_o} + \frac{2}{\rho}\int_o^{x_o} \bar{\tau}_w\, \frac{h_s}{B}\, \frac{dx}{x_o} \quad \beta U_{i1}^2\, \frac{h_{s1}}{x_o} \tag{54}$$

This last relation can be obtained also by applying the momentum principle to the entire body of the salt wedge at the instant t and contained in the boundary ADCB as shown in Figure 10. Let the rate of change of

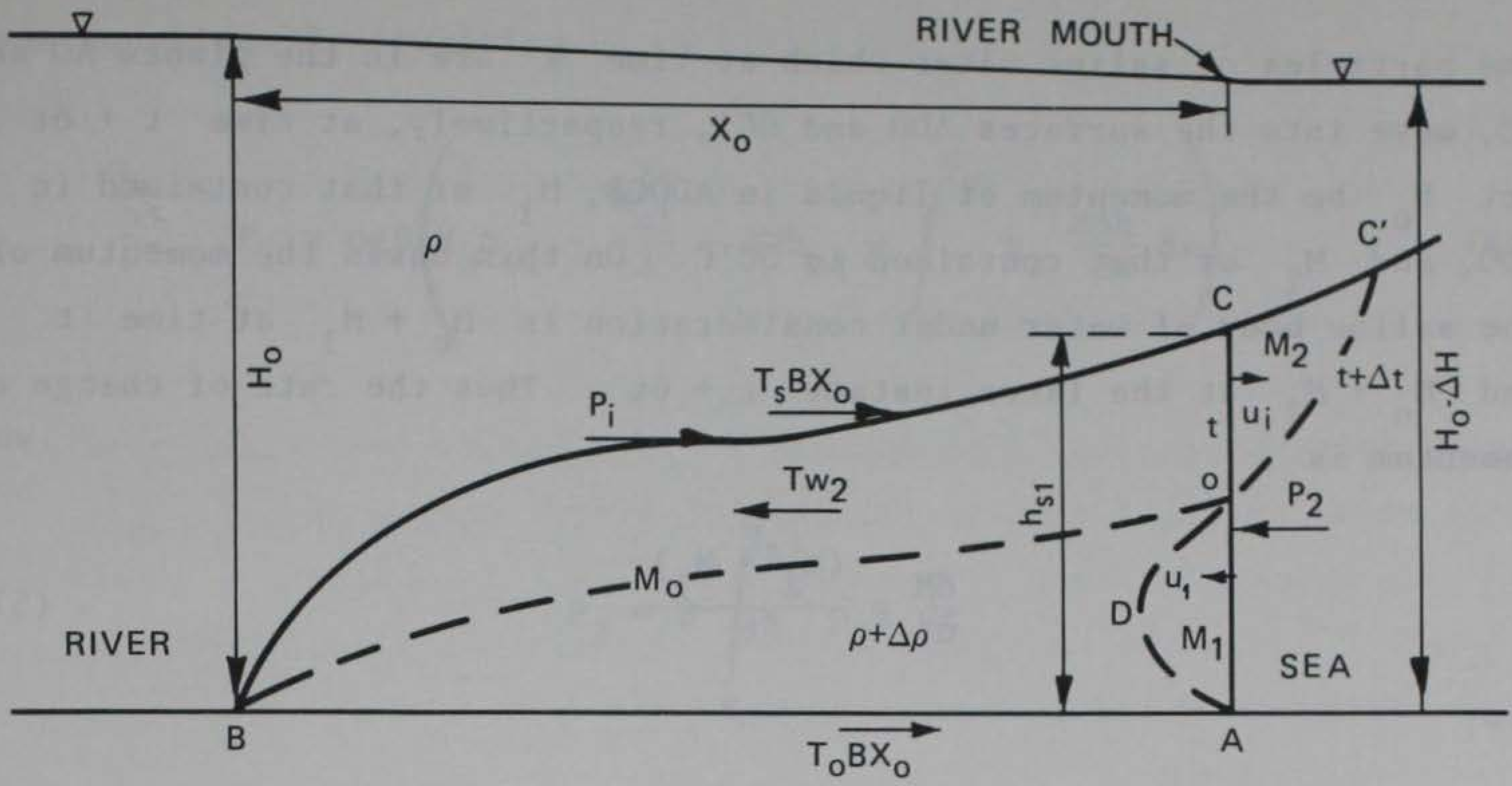

Figure 10. Notation diagram relating to momentum of salt wedge

momentum of this body of liquid in the direction of x positive be denoted by

$$\frac{\delta M}{\delta t}$$

The forces producing this change are the total pressure forces P_i acting on the interface and P_2 acting on the limiting face of the saline wedge with the depth h_{s1}. The tractive forces also taking part in this are the interfacial total stress $T_s Bx_o$ and the retarding force of the sidewalls T_{w2}.

Thus

$$\frac{\delta M}{\delta t} = P_i - P_2 + T_s Bx_o + T_o Bx_o - T_{w2} \tag{55}$$

In the notation previously adopted

$$T_{w2} = 2 \int_0^{x_o} \bar{\tau}_w h_s \, dx \tag{56}$$

The particles of saline water which at time t are in the planes AO and OC, move into the surfaces ADO and OC', respectively, at time $t + \delta t$. Let M_o be the momentum of liquid in ADOCB, M_1 of that contained in ADO, and M_2 of that contained in OC'C. On this basis the momentum of the saline body of water under consideration is $M_o + M_1$ at time t and $M_o + M_2$ at the later instant $t + \delta t$. Thus the rate of change of momentum is

$$\frac{\delta M}{\delta t} = \frac{(M_2 - M_1)}{\delta t} \tag{57}$$

Now,

$$M_1 = -\rho B \int_o^{\delta} \int_{-b}^{+b} u_1^2 \, dz \, dy \, \delta t$$

and

$$M_2 = \rho B \int_{\delta}^{h_{s1}} \int_{-b}^{+b} u_1^2 \, dz \, dy \, \delta t$$

as u_1 is negative for z smaller than δ, and positive for z greater than δ. Substituting in Equation 53

$$\frac{\delta M}{\delta t} = B\rho \int_o^{h_{s1}} \int_{-b}^{+b} u_1^2 \, dx \, dy \tag{58}$$

and in agreement with Equation 47, $A = h_{s1}B$

$$\frac{\delta M}{\delta t} = \beta U_i^2 h_{s1} B \tag{59}$$

From Equation 39, rewriting

$$P_i = \rho g B\left(H_o h_{s1} - \frac{h_{s1}^2}{2} - \Delta H h_{s1} + \int_o^{x_o} h_s \frac{d\Delta h}{dx} dx\right) \qquad (60)$$

Now

$$P_2 = B \int_o^{h_{s1}} p_2 z \, dz$$

where

$$p_2 = \rho g \, (H_o - \Delta H - h_{s1}) + g(\rho + \Delta\rho) \, h_{s1} - g(\rho + \Delta\rho) \, z$$

The integration yields

$$P_2 = \rho g B\left(H_o h_{s1} - \Delta H h_{s1} - \frac{h_{s1}^2}{2} + \frac{\Delta\rho}{\rho} \frac{h_{s1}^2}{2}\right) \qquad (61)$$

Substituting in Equation 51 from Equations 59, 60, and 61 and dividing by $\rho B x_o$, results in

$$\frac{T_s}{\rho} + \frac{T_o}{\rho} = -g \int_o^{x_o} h_s \frac{d\Delta h}{dx} \frac{dx}{x_o} + \frac{g}{2} \frac{\Delta\rho}{\rho} \frac{h_{s1}^2}{x_o} + \frac{2}{\rho B} \int_o^{x_o} \bar{\tau}_w h_s \frac{dx}{x_o} + \beta U_{i1}^2 \frac{h_{s1}}{x_o} \qquad (62)$$

which agrees with Equation 54, since $h = H_o - \Delta h$.

PART IX: DIMENSIONLESS FORM OF THE STRESS EQUATIONS

34. In evaluating the average interface and bottom stresses on the basis of Equations 32 and 50 using experimental data, it will be useful first to express these equations in a dimensionless form. It is further required that the average resistive stress $2\bar{\tau}$ on the channel walls, from fresh water and saline water, be ascertained analytically since these stresses are not amenable to direct measurements.

35. In laboratory experiments the Reynolds number of flow accounted is generally small and hence the resistance of the sidewalls may be determined by the Blasius relation

$$\frac{\bar{u}}{u_*} = a\left(\frac{u_* b}{\nu}\right)^{1/7} \quad , \; a = 7.64 \tag{63}$$

where $u_* = (\tau/\rho)^{1/2}$ and $\bar{u}$ is the mean velocity at points having a constant distance z' from the interface. From this

$$\frac{\tau}{\rho} = a_1\left(\frac{\bar{u}b}{\nu}\right)^{-1/4} \bar{u}^2 \quad , \; a_1 = 0.0284$$

and

$$\frac{\tau}{\rho U^2} = a_1 \left(\frac{Ub}{\nu}\right)^{-1/4} \left(\frac{\bar{u}}{U}\right)^{7/4}$$

where U is the average velocity of the fresh water in a section. Then for the average shear on the wall

$$\frac{\bar{\tau}}{\rho U^2} = a_1\left(\frac{Ub}{\nu}\right)^{-1/4} \int_0^1 \left(\frac{\bar{u}}{U}\right)^{7/4} ds \quad , \; s = \frac{z'}{h_w}$$

z' is distance measured from the interface and h_w is the depth of fresh water. First affecting the integration on the basis of data shown in Table 11, one then has, after introducing U_o, the river mean velocity,

$$\frac{2\bar{\tau}}{\rho U_o^2} = \lambda_o \left(\frac{U}{U_o}\right)^{7/4} \tag{64}$$

where

$$\lambda_o = 0.051 \left(\frac{U_o b}{\nu}\right)^{-1/4} \tag{65}$$

This estimate is only provisional as it assigns a larger value to the resistance. The derivation ignores the effects of turbulence of the free surface and of the interface. At such points one expects lower stresses than assumed. In the saline water area the frictional effect of the wall is not very critical. Since in one part motion is directed toward the sea and in the other part away from the sea, resistance effects are somewhat neutralized. As the application of the above method to this case is less likely to be valid, it is better to ignore it for the present.

36. Dividing Equation 32 by U_o^2, the result is

$$\frac{T_s}{\rho U_o^2} = \frac{gH_o}{U_o^2}\frac{\Delta H}{x_o} I_1 - \alpha \frac{H_o}{x_o} I_2 - \lambda_o \frac{H_o}{B} I_3 \tag{66}$$

where

$$I_1 = 1 - n\int_o^1 \frac{h_s}{h_{s1}} \frac{d(dh/\Delta H)}{d\zeta} d\zeta \ , \ n = \frac{h_{s1}}{H_o}$$

$$I_2 = \frac{h_{s1} + \Delta H}{(H_o - \Delta H - h_{s1})} = \frac{h_{s1}}{H_o - h_{s1}}$$

and

$$I_3 = \int_o^1 \left(\frac{U}{U_o}\right)^{-7/4} \left(\frac{h - h_s}{H_o}\right) d\zeta = \int_o^1 \left(1 - n\,\frac{h_s}{h_{s1}}\right)^{-3/4} d\zeta \tag{67}$$

Utilizing the experimental values of h_s/h_{s1} and $\Delta h/\Delta/H$ expressed in terms of ζ , see Equations 12 and 15, and affecting the integration and remembering that $n = h_{s1}/H_o$, the above given multipliers are

$$I_1 = 1 - 0.59n \tag{68}$$

$$I_2 = n/(1 - n) \tag{69}$$

$$I_3 = 1 + 0.37n + 0.20n^2 \tag{70}$$

37. Dividing Equation 54 by U_o^2 , ignoring the small value term from the sidewall fraction, the result is

$$\frac{T_o}{\rho U_o^2} + \frac{T_s}{\rho U_o^2} = -n\,\frac{gH_o}{U_o^2}\,\frac{\Delta H}{x_o}\,I_4 + \frac{n}{2}\,\frac{gH_o}{U_o^2}\,\frac{\Delta\rho}{\rho}\,\frac{h_{s1}}{x_o} + I_5\,\frac{H_o}{x_o} \tag{71}$$

where

$$I_4 = \int_o^1 \frac{d(\Delta h/\Delta H)}{d\zeta}\,\frac{h_s}{h_{s1}}\,d\zeta = 0.59 \tag{72}$$

$$I_5 = \beta\left(\frac{U_{i1}}{U_1}\right)^2 \frac{n}{(1 - n)^2}$$

The definition of the Boussinesq velocity coefficients α is given by

Equation 23 and that of β by Equation 47. These coefficients may be evaluated through the entries of the last columns in Tables 10 and 11, respectively. It will be remembered that these tables give the root-mean-square values of velocity u of points of as common distance z' from the interface in a given cross section. This fact is due to the manner in which the determinations are made. The hydrodynamic forces acting on the ribbon and causing it to deflect are proportional in the square of the velocity of the particles striking the ribbon. With this interpretation

$$\alpha = 1.012 \tag{73}$$

and

$$\beta = 0.14 \tag{74}$$

since $U_{i1}/U_1 = 0.53$ and $\beta = 0.14$ the last multiplier reduces to

$$I_5 = \frac{0.033n}{(1 - n)^2} \tag{75}$$

Accordingly, after neglecting the term involving λ , representing the effect of wall friction the final form of the equation to evaluate the average bottom shear is

$$\frac{T_o}{\rho U_o^2} + \frac{T_s}{\rho U_o^2} = n \frac{gH_o}{U_o^2} \left(-0.59 \frac{\Delta H}{x_o} + \frac{1}{2} \frac{\Delta \rho}{\rho} \frac{h_{s1}}{x_o} \right) + \frac{0.033n}{(1 - n)^2} \tag{76}$$

Subtracting Equation 64 from this last equation and recalling that $I_1 = 1 - 0.59n$, the result is

$$\frac{T_o}{\rho U_o^2} = \frac{gH_o}{U_o^2} \left(- \frac{\Delta H}{x_o} + \frac{n}{2} \frac{\Delta \rho}{\rho} \frac{h_{s1}}{x_o} \right) + \alpha \frac{H_o}{x_o} I_2 + \lambda_o \frac{H_o}{B} I_3 + I_5 \frac{H_o}{x_o} \tag{77}$$

It is preferable to use this equation to evaluate the average bottom stress under the arrested saline wedge.

PART X: EXPERIMENTAL VALUES OF INTERFACIAL STRESS

38. Using Equations 66 and 77 the experimental values of average interfacial stress T_s and average bottom stress under the wedge T_o are evaluated on the basis of data shown in Tables 1 and 2. The evaluation as function of U_oH_o/ν are collected in Tables 12 and 13 for water depth $H_o = 23.0$ cm and 45.5 cm, respectively. Since the values thus arrived should be independent of the ratio H/B, the values of T_s and T_o for the two depths are shown in Figures 11 and 12. Here, $2T_s/\rho U_o^2$ is plotted logarithmically against U_oH_o/ν and also $2T_o/\rho U_o^2$ against U_oH_o/ν. The scatter of the points in both figures is very large. This is hardly surprising and was expected since the values of T_s and T_o are obtained in both cases by subtracting quantities of nearly equal order of magnitude, each of these quantities separately being open to errors as large as 5 percent. In particular, the fall of water surface ΔH cannot be determined with certainty. In this study ΔH is not measured directly; it is deduced from a curve of observed points $\Delta h'$ versus x and there is an element of subjectivity. Another cause for the scatter is the fact that the points of the figures as regards to n are not comparable. By dimensional analysis it may be shown that

$$\frac{2T_s}{\rho U_o^2} = f_1\left(\frac{U_oH_o}{\nu}\ ,\ n\right) \tag{78}$$

and

$$\frac{2T_o}{\rho U_o^2} = f_2\left(\frac{U_oH_o}{\nu}\ ,\ n\right) \tag{79}$$

For the data shown in the figures n is not constant but varies from 0.35 to 0.55. A good average value of n for all the points is $n = 0.45$. In Figure 11 a straight line is drawn through the points, with a slope equaling 1. Half of the observed points are above the line and the other half below the line; and judging by the eye, the

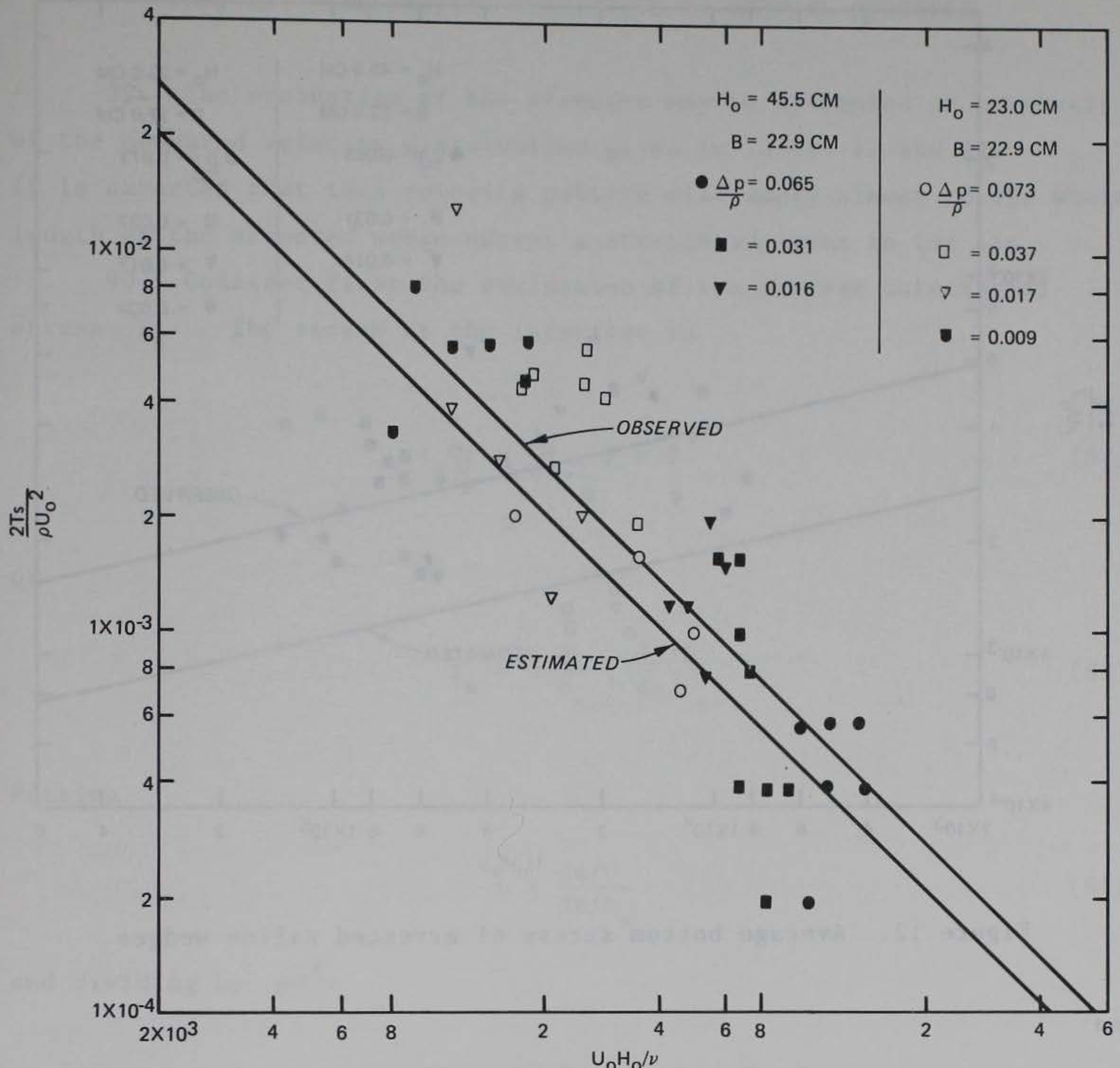

Figure 11. Average interfacial stress of arrested saline wedge

squares of the deviations are at their least value. In Figure 12, the slope of the straight line drawn through the points equals 1/4. Accordingly the average stresses are

$$\frac{2T_s}{\rho U_o^2} = 54\left(\frac{U_o H_o}{\nu}\right)^{-1}, \; n = 0.45 \tag{80}$$

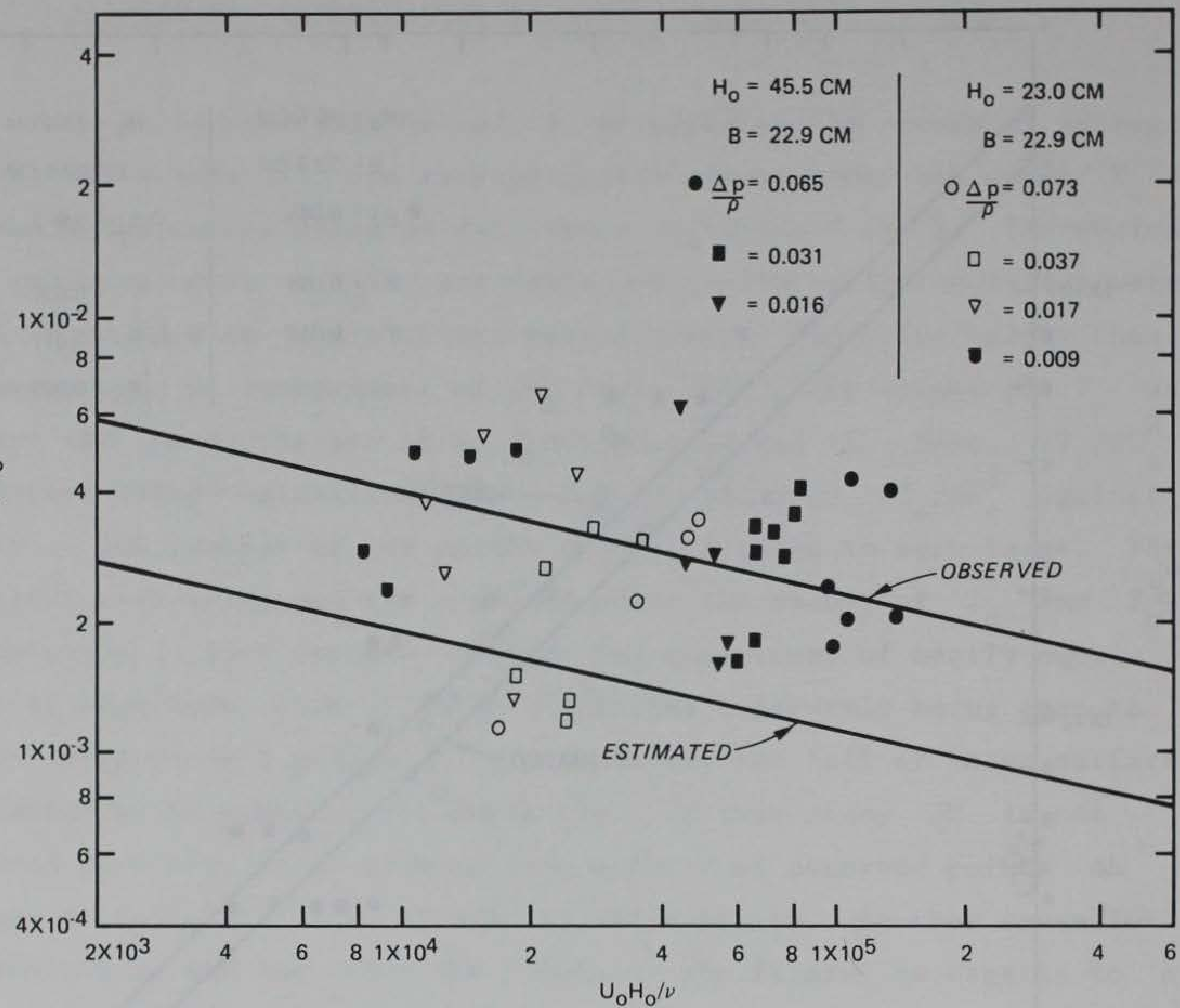

Figure 12. Average bottom stress of arrested saline wedges

and

$$\frac{2T_o}{\rho U_o^2} = 0.03 \left(\frac{U_o H_o}{\nu} \right)^{-1/4} , \; n = 0.45 \tag{81}$$

The examined data cover the range of Reynolds number $R = 4{,}000$ to $R = 110{,}000$. These are in agreement with the previous investigation (Keulegan 1957b) excepting a slight decrease in T_o .

PART XI: THEORETICAL EVALUATION OF AVERAGE STRESSES

39. The evaluation of the stresses may be attempted on the basis of the measured velocity distribution given in Tables 10 and 11. It is expected that this velocity pattern will apply almost to the whole length of the arrested wedge except a stretch adjacent to the tip.

40. Consider first the evaluation of the average interfacial stress T_s. The stress at the interface is

$$\tau_s = \mu \frac{du}{dz} , \; z = 0 \tag{82}$$

or

$$\tau_s = \mu \frac{U}{h_s} , \; \frac{du/U}{dz/h_s} \tag{83}$$

Putting

$$m = \frac{du/U}{dz/h_s} \tag{84}$$

and dividing by $\rho U^2{}_o$

$$\frac{\tau_s}{\rho U_o^2} = m \left(\frac{U_o H_o}{\nu} \right)^{-1} \times \frac{U}{U_o} \frac{H_o}{h_s}$$

Remembering that $n = h_{s1}/H_o$

$$\frac{\tau_s}{\rho U_o^2} = m \left(\frac{U_o H_o}{\nu} \right)^{-1} \frac{1}{n} \frac{U}{U_o} \frac{h_{s1}}{h_s}$$

Introducing the average shear T_s

$$\frac{T_s}{\rho U_o^2} = 2m \left(\frac{U_o H_o}{\nu}\right)^{-1} \frac{1}{n} \int_{\varepsilon}^{1} \frac{d\zeta}{\frac{h_s}{h_{s1}}\left(1 - n\frac{h_s}{h_{s1}}\right)} \tag{85}$$

Placing

$$F_1 = \frac{1}{n} \int_{\varepsilon}^{1} \frac{d\zeta}{\frac{h_s}{h_{s1}}\left(1 - n\frac{h_s}{h_{s1}}\right)} \tag{86}$$

one now has

$$\frac{2T_s}{\rho U_o^2} = 2mF_1\left(\frac{U_o H_o}{\nu}\right)^{-1} \tag{87}$$

Taking h_s/h_{s1} from Table 4, F_1 is computed by numerical integration for a few selected values of ε and n . These values are given in Table 14.

41. Toward the evaluation of the factor m one needs to consider the velocity rates in the area of the interface. The appropriate quantities are taken from the entries of Tables 10 and 11 and are shown in graph form in Figure 13. The inclinations of the straight lines, one for the region of the fresh water and the other for the salt water, are somewhat different in value; this is in accordance with the fact that the viscosity of salt water is somewhat greater than that of fresh water. On the basis of these data the factor m amounts to 3.0. As the average value of n of all the tests is 0.45, the corresponding F_1 is read from Table 14 and for an assumed ε , equal to 0.05, is 6.53. Substitution of these in Equation 87 yields for the average interfacial stress the result

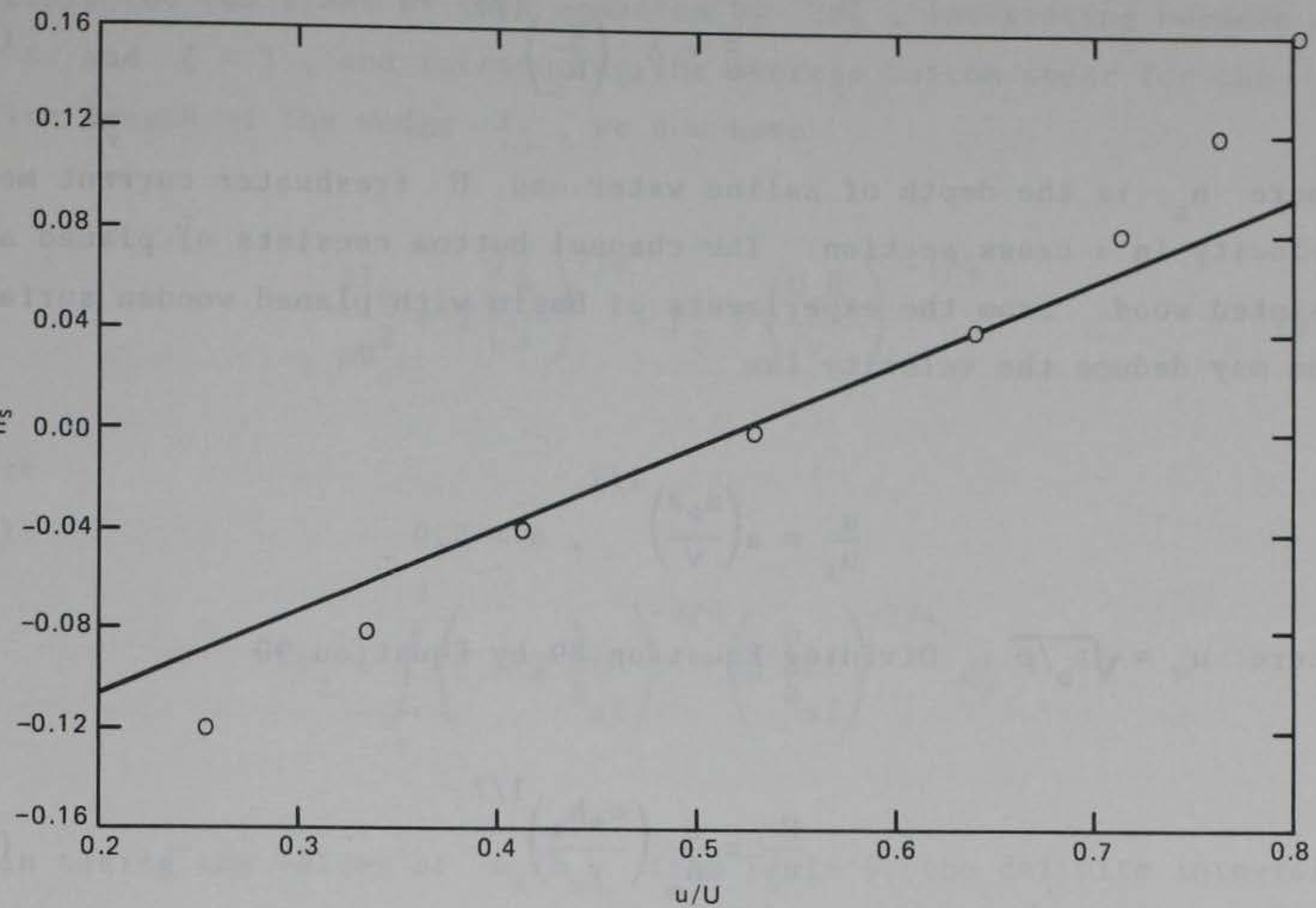

Figure 13. Interface velocity gradient

$$\frac{2T_s}{\rho U_o^2} = 39 \left(\frac{U_o H_o}{\nu} \right)^{-1} \tag{88}$$

The plot of this relation is shown in Figure 11. Agreement between the theory and the observation is quite fair.

42. Although a slight mixing is present between fresh and saline waters, this fact fails to destroy the effective laminar regime of the interface. However, one expects the initiation of a turbulent regime for high Reynolds number, but the present tests fail to give any indication of the exact value of $U_o H_o/\nu$ needed. The maximum $U_o H_o/\nu$ noted is 1.2×10^5.

43. Flow in the saline water close to the bottom is turbulent. As the Reynolds number of flow is small, according to Blasius' hypothesis the velocities would vary as the one-seventh power of distance from bottom. Thus, one expects that

$$\frac{u}{U} = A_o \left(\frac{z}{h_s}\right)^{1/7} \tag{89}$$

where h_s is the depth of saline water and U freshwater current mean velocity in a cross section. The channel bottom consists of planed and painted wood. From the experiments of Bazin with planed wooden surfaces one may deduce the velocity law

$$\frac{u}{u_*} = a\left(\frac{u_* z}{\nu}\right)^{1/7} \quad , \; a = 5.9 \tag{90}$$

where $u_* = \sqrt{\tau_o/\rho}$. Dividing Equation 89 by Equation 90

$$\frac{U}{u_*} = \frac{a}{A_o}\left(\frac{u_* h_s}{\nu}\right)^{1/7} \tag{91}$$

Solving for τ_o ,

$$\tau_o = \left(\frac{a}{A_o}\right)^{-7/4} \left(\frac{h_s}{\nu}\right)^{-1/4} U^{7/4} \tag{92}$$

or

$$\frac{\tau_o}{\rho U_o^2} = \left(\frac{a}{A_o}\right)^{-7/4} \left(\frac{U_o H_o}{\nu}\right)^{-1/4} \left(\frac{U}{U_o}\right)^{-7/4}$$

Introducing $U_o H_o = U(H_o - h_s)$ and putting $h_{s1} = nH_o$ one obtains

$$\frac{\tau_o}{\rho U_o^2} = \left(\frac{a}{A}\right)^{-7/4} \left(\frac{U_o H_o}{\nu}\right)^{-1/4} \left(n\,\frac{h_s}{h_{s1}}\right)^{-1/4} \left(1 - n\,\frac{h_s}{h_{s1}}\right)^{-7/4}$$

Multiply the two sides of this equation by $2d\zeta$, integrating between $\zeta = \varepsilon$ and $\zeta = 1$, and introducing the average bottom shear for the entire length of the wedge T_o, we now have

$$\frac{2T_o}{\rho U_o^2} = 2\left(\frac{A_o}{a}\right)^{7/4} \cdot F_2 \cdot \left(\frac{U_o H_o}{\nu}\right)^{-1/4} \tag{93}$$

where

$$F_2 = \int_{\varepsilon}^{1} \left(1 - n\frac{h_s}{h_{s1}}\right)^{-7/4} \left(n\frac{h_s}{h_{s1}}\right)^{-1/4} d\zeta$$

Again taking the values of h_s/h_{s1} from Table 4, the definite integral may be computed by numerical integration for selected values of n and ε. These are given in Table 15.

44. The examination of lower velocities of the arrested saline wedge shown in Figure 7 suggests that A_o equals 0.25. Selecting $\varepsilon = 0.05$ and $n = 0.45$, Table 15 gives $F_2 = 2.3$. As indicated in the above, $a = 5.9$. Inserting these in Equation 73, the result is

$$\frac{2T_o}{\rho U_o^2} = 0.018\left(\frac{U_o H_o}{\nu}\right)^{-1/4} \tag{94}$$

This is plotted in Figure 12. The estimated values of T_o are twice as small as the values obtained from Equation 73. Probably the main reason for this large difference was the obvious difficulty of measuring small velocities accurately. In the derivation above it was assumed tacitly that there is similarity in velocity pattern. In the presence of mixing at the interface this assumption would not be valid, and the evaluation should be carried out on a different basis.

PART XII: DISCUSSIONS

A Theory of Affine Shape of Arrested Saline Wedge

45. In a study dealing with the circulation of cooling water between the intake and the outlet of a thermoelectric power plant Beta (1957) has shown that the affine shape of an arrested wedge computed from the flow equations originally given by Shijf and Schoenfeld (1953), is in agreement with observations. Comparison with theory is made also for observations from Keulegan (1952) covering the range from $F_o = 0.06$ to $F_o = 0.40$. These fall on the theoretical curve corresponding to $F_o = 0.55$. Later, using a similar analysis, Harleman (1961) has indicated that there is agreement between theory and observation as regards the shape of arrested saline wedges. These are significant findings and require further consideration.

46. The equation of motion as relating to the freshwater layer above the saline wedge may be obtained directly from Equation 30. Neglecting the wall friction τ_w , taking x equal to unity, writing h_w for $h - h_s$, the desired result is

$$\frac{dh}{dx} + \frac{U}{g}\frac{dU}{dx} = -\frac{\tau_s}{g\rho h_w} \tag{95}$$

From Equation 48 neglecting bottom friction τ_o and placing $\beta = 0$ (no motion in the wedge) one has

$$\frac{dh}{dx} + \frac{\Delta\rho}{\rho}\frac{dh_s}{dx} = \frac{\tau_s}{\rho g h_s} \tag{96}$$

as relating to a stationary salt wedge. These agree with the equations of Shijf and Schoenfeld (1953). Because of the condition of continuity

$$U\frac{dh_w}{dx} = -h_w\frac{dU}{dx} \tag{97}$$

and assuming that the fall of surface water may be neglected

$$\frac{dh_w}{dx} = - \frac{dh_s}{dx} \tag{98}$$

and then

$$U \frac{dh_s}{dx} = h_w \frac{dU}{dx}$$

Introducing the latter in Equation 95,

$$\frac{dh}{dx} + \frac{U^2}{gh_w} \frac{dh_s}{dx} = - \frac{\tau_s}{\rho g h_w} \tag{99}$$

Subtracting Equation 99 from Equation 96, the result is

$$\left(\frac{\Delta\rho}{\rho} - \frac{U^2}{gh_w} \right) \frac{dh_s}{dx} = \frac{\tau_s}{\rho g} \left(\frac{1}{h_w} + \frac{1}{h_s} \right) \tag{100}$$

Introducing

$$\frac{\tau_s}{\rho} = \frac{\lambda_i U^2}{2} \tag{101}$$

Equation 100 becomes

$$\left(\frac{\Delta\rho}{\rho} - \frac{U^2}{gh_w} \right) \frac{dh_s}{dx} = \frac{\lambda_i}{2} \frac{U^2}{g} \left(\frac{1}{h_w} + \frac{1}{h_s} \right)$$

which may be written also as

$$\left[\frac{\Delta\rho}{\rho} - \frac{U_o^2}{gH_o} \left(\frac{U}{U_o} \right)^2 \frac{H_o}{h_w} \right] \frac{dh_s}{dx} = \frac{\lambda_i}{2} \frac{U_o^2}{gH_o} \left(\frac{U}{U_o} \right)^2 \left(\frac{H_o}{h_w} + \frac{H_o}{h_s} \right) \tag{102}$$

Placing

$$\eta = \frac{h_s}{H_o} \quad ; \; s = \frac{x}{H_o} \tag{103}$$

and as, neglecting Δh ,

$$\frac{U_o}{U} = 1 - \eta$$

in terms of new variables Equation 98 changes to

$$\left[\eta(1 - \eta)^3 - F_o^2 \eta \right] d\eta = \frac{\lambda_i}{2} F_o^2 \; ds \tag{104}$$

Here F_o is the densimetric Froude number

$$F_o = V_r / V_\Delta = \frac{U_o}{\left(\frac{\Delta\rho}{\rho} \; gH_o \right)^{1/2}}$$

The solution of Equation 100 subject to the condition $\eta = 0$ at $s = 0$, is

$$\left(1 - F_o^2\right) \frac{\eta^2}{2} - \eta^3 + \frac{3}{4} \eta^4 - \frac{\eta^5}{5} = \frac{\lambda_i}{2} F_o^2 \cdot \frac{x}{H_o} \tag{105}$$

Replacing x by x_o , the length of the arrested saline wedge, and η by η_L ,

$$\eta_L = \frac{h_{s1}}{H_o}$$

one also has

$$\left(1 - F_o^2\right) \frac{\eta_L^2}{2} - \eta_L^3 + \frac{3}{4} \eta_L^4 - \frac{1}{5} \eta_L^5 = \frac{\lambda_i}{2} F_o^2 \frac{x_o}{H_o} \tag{106}$$

This may be written after placing

$$\phi(\eta_L) = \left(1 - F_o^2\right)\frac{\eta_L^2}{2} - \eta_L^3 + \frac{3}{4}\eta_L^4 - \frac{1}{5}\eta_L^5 \qquad (107)$$

as

$$\phi(\eta_L) = \frac{\lambda_i}{2} F_o^2 \frac{x_o}{H_o} \qquad (108)$$

Here is an expression which relates the coefficient of resistance of the interface with the length of the arrested wedge. It is equivalent to one already indicated by Harleman (1961). It is valid only in the case where the bottom stress vanishes and the momentum of the wedge can be ignored. Now, dividing Equation 105 by Equation 108 and writing $\zeta = x/x_o$, as before, one has

$$\left(1 - F_o^2\right)\frac{\eta^2}{2} - \eta^3 + \frac{3}{4}\eta^4 - \frac{\eta^5}{5} = \phi(\eta_L)\cdot\zeta \qquad (109)$$

Assuming that the flow at the river mouth is critical

$$\eta_L = 1 - F_o^2 \qquad (110)$$

We note also that

$$\eta = \frac{h_s}{h_{s1}}\eta_L \qquad (111)$$

Thus, through Equations 105, 106, and 107, ζ may be obtained as a function of h_s/h_{s1} for a chosen F_o. A few determinations are shown in Figure 14. The circles represent experimental values for an F of 0.40 and are taken from Table 5. Agreement between the theoretical values and the observations is good. In the experimental wedges friction is present at the flume walls and also at the wedge bottom. In the

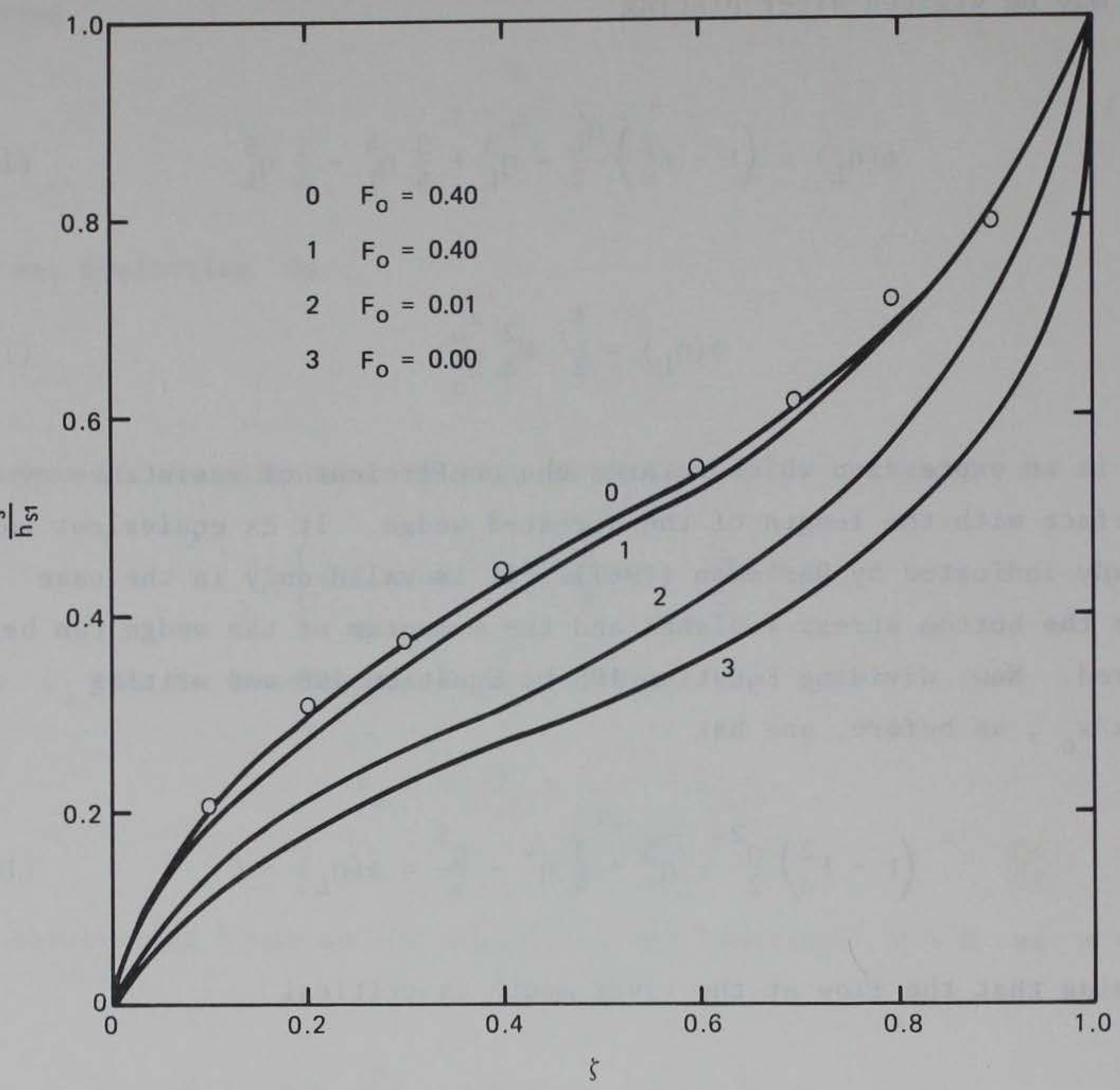

Figure 14. Theoretical affine shape of arrested wedges

theoretical evaluations these frictions are ignored. The observed close agreement could be hardly expected, unless these two frictions are of like value and may be imagined to be incorporated into the interfacial stress τ_s . Another point to remember is that the critical flow condition at the river mouth, Equation 110, is valid only for values of F_o close to 0.5. Variation from the expression becomes important as F_o approaches zero. In the usual derivation, it is assumed tacitly that at the river mouth the pressure is hydrostatic. When the depth of salt wedge at the river mouth is increased the interface tends to be more curved, affecting the pressure there, and this is no longer hydrostatic. The

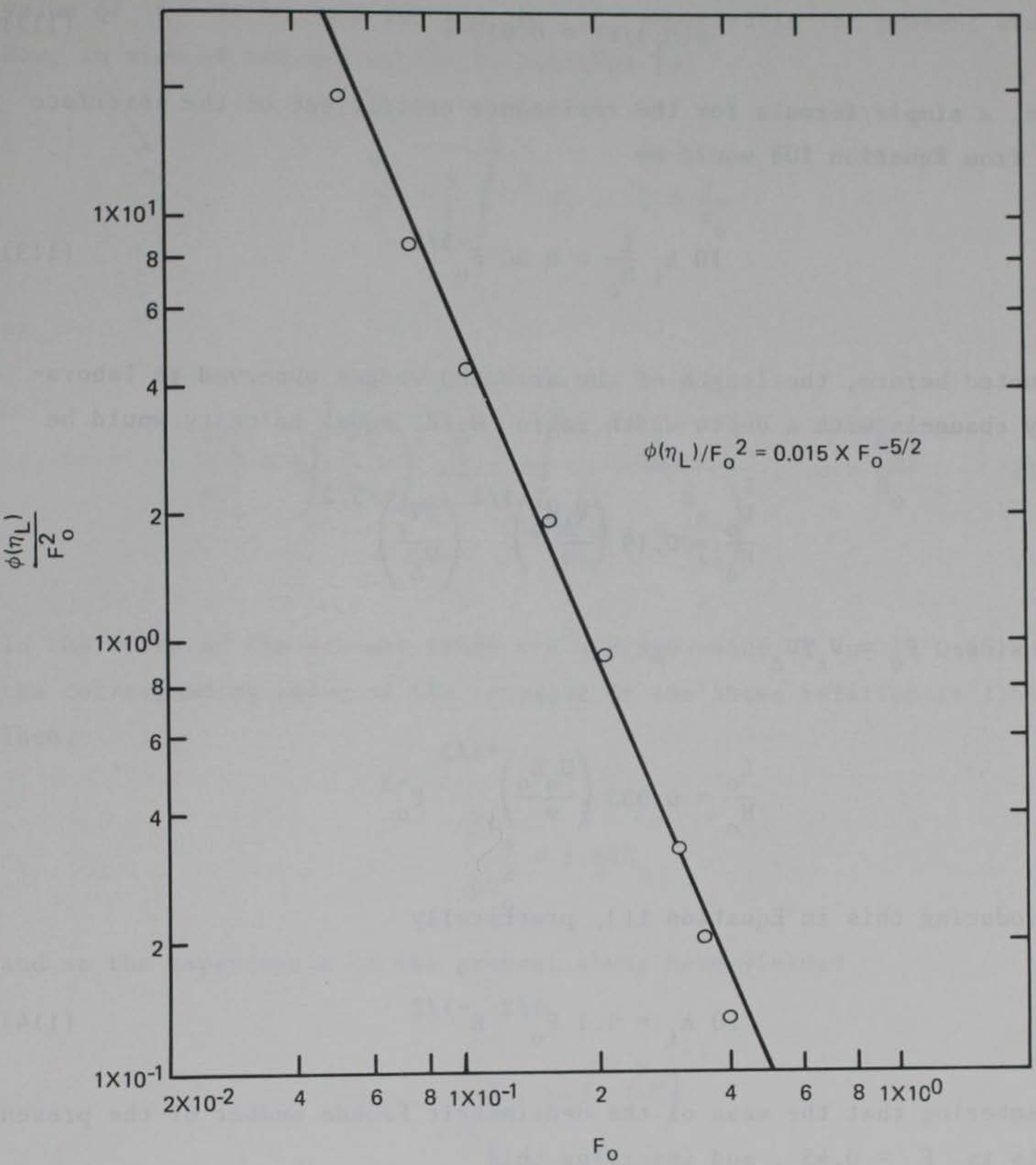

Figure 15. Dependence of ϕ on F_o

critical conditions are not exactly known and experimental elucidation of the matter is very much desired. This was mentioned before.

47. Equation 108 relates the length of arrested saline wedge to the friction coefficient of the interface λ_i. The quantity $\phi(\eta_L)$ is plotted against F_o in Figure 15. For the range between $F_o = 0.5$ and $F_o = 0.1$ a good approximation for $\phi(\eta_L)$ is

$$\phi(\eta_L)/F_o^2 = 0.015\ F_o^{-5/2} \tag{112}$$

Thus, a simple formula for the resistance coefficient of the interface λ_i from Equation 108 would be

$$10\ \lambda_i \frac{L}{H_o} = 0.30\ F_o^{-5/2} \tag{113}$$

As noted before, the length of the arrested wedges observed in laboratory channels with a depth width ratio H_o/B equal to unity would be

$$\frac{L_o}{H_o} = 0.19 \left(\frac{V_\Delta H_o}{\nu}\right)^{1/2} \left(\frac{2V_r}{V_\Delta}\right)^{-5/2}$$

or, since $F_o = V_r/V_\Delta$

$$\frac{L_o}{H_o} = 0.033 \left(\frac{U_o H_o}{\nu}\right)^{+1/2} F_o^{-3}$$

Introducing this in Equation 113, practically

$$10\ \lambda_i = 9.1\ F_o^{1/2}\ R^{-1/2} \tag{114}$$

Remembering that the mean of the densimetric Froude number of the present tests is $F_o = 0.45$, and inserting this

$$10\ \lambda_i = 6.1\ (U_o H_o/\nu)^{-1/2} \tag{115}$$

48. This would be the value of the coefficient on the basis of the length of wedges observed in the laboratory channels and the theoretical relation between the coefficient and the length of the wedge, Equation 108.

49. It would be of interest to compare the above result with the

value of λ_i to be deduced from the T_s observed in the present study. Now, in view of the definition in Equation 101

$$\frac{T_s}{\rho} = \frac{\lambda}{2} \int_o^1 U^2 \, d\zeta \ , \quad \zeta = \frac{x}{x_o}$$

or

$$\frac{2T_s}{\rho U_o^2} = \lambda \int_o^1 \left(\frac{U}{U_o}\right)^2 d\zeta = \lambda \int_o^1 \frac{d\zeta}{\left(1 - n \, \frac{h_s}{h_{s1}}\right)^2} \ , \quad n = \frac{h_{s1}}{H_o} \qquad (116)$$

In the tests of the present study the average value of n is 0.45 and the corresponding value of the integral in the above relation is 1.64. Then,

$$\frac{2T_s}{\rho U_o^2} = 1.64\lambda$$

and as the experiments of the present study here yielded

$$\frac{2T_s}{\rho U_o^2} = 54 \left(\frac{U_o H_o}{\nu}\right)^{-1}$$

the equation of the upper line in Figure 11, we have

$$\lambda_i = 32.9 \left(\frac{U_o H_o}{\nu}\right)^{-1} \qquad (117)$$

a result not in agreement with Equation 115. At the moment we are unable to discuss the reason for this difference.

50. In a definitive study the nature of interfacial stress in lock exchange was examined by Abraham and Eyesink (1971). The coefficient of stress λ_i may be defined as

$$\tau_i = \frac{\lambda_i}{2} \rho U_r^2 \tag{118}$$

where U_r is the relative velocity between the two layers of the exchange flow and τ_i the interface stress. Authors use the Weisbach coefficient f , $f = 4\lambda_i$. Resorting to an energy consideration, $4\lambda_i$ is first evaluated utilizing the experimental data of Keulegan (1957a) and Barr (1963) on exchange flow involving laboratory flumes. To examine the effect of viscosity on the coefficient these authors performed additional experiments in two channels, one small and the other 3.45 times as great in the Delft Hydraulics Laboratory. Evaluation of the coefficient is effected using the flow equations originally formulated by Shijf and Schoenfeld (1953). Initial conditions only are considered coinciding with the densimetric Froude number $F_r = 0.9$, the number being defined

$$F_r = \frac{U_r}{\sqrt{\frac{\Delta\rho}{\rho g H_o}}} \tag{119}$$

H_o being the combined depth of the two layers. The authors present the evaluations of the coefficient as a function of Reynolds number

$$R_e = \frac{U_2 R_2}{\nu} \tag{120}$$

where U_2 is the current velocity in the lower layer and R_2 is the hydraulic radius

$$R_2 = \frac{h_s B}{2(h_s + B)} \qquad (121)$$

where h_s is the depth of the lower layer and B the width of channel. As the depth of water H_o equals $2h_s$

$$h_s = \left(2 + \frac{H_o}{B}\right) R_2 \qquad (122)$$

For the present purpose it is desirable to express the coefficient as a function of the Reynolds number $U_2 h_s/\nu$. The authors' data may be readily expressed as a function of $U_2 h_s/\nu$ as well. This is done in Figure 16. Results from the authors' experiments are in agreement with

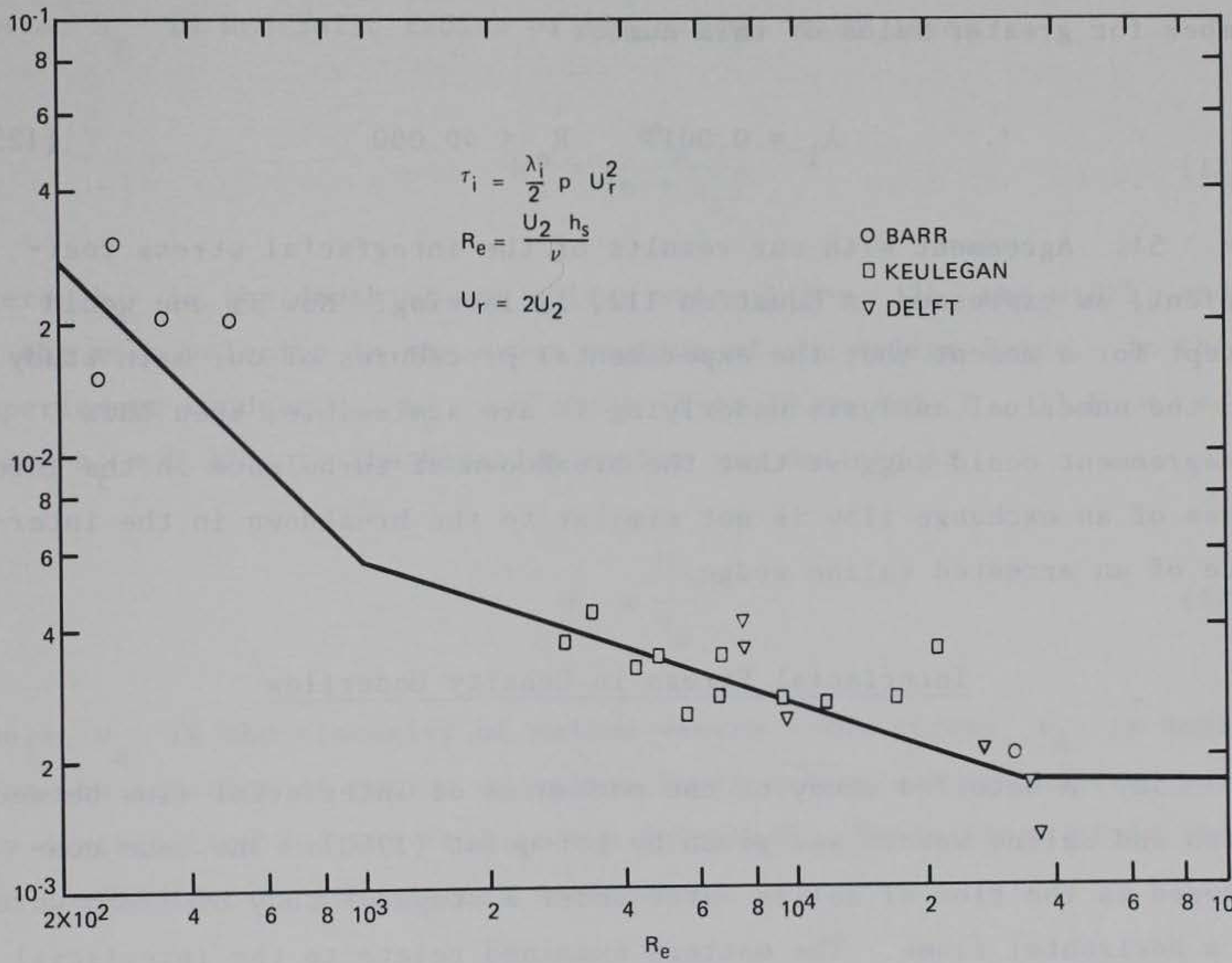

Figure 16. Relation between λ_1 and R_e in exchange flow (after Abraham and Eyesink 1971)

the evaluation from the Barr and Keulegan data. Three distinct regions are discernible. In the laminar range

$$\lambda_i = 5.5R_e^{-1} \qquad R_e < 1000 \tag{123}$$

This is also the relation derived by Ippen and Harleman (1952) for the case of an underflow, that is, flow of saline waters in an incline under a stagnant pool of fresh water. In the transition range

$$\lambda_i = 0.055R_e^{-1/3} \qquad 1000 < R_e < 40.000 \tag{124}$$

The authors point out that the coefficient is independent of Reynolds number for greater value of this number

$$\lambda_i = 0.0017 \qquad R_e < 40.000 \tag{125}$$

51. Agreement with our results of the interfacial stress coefficient, as expressed in Equation 112, is lacking. Now if one would accept for a moment that the experimental procedures of our main study and the numerical analysis underlying it are admissible, then this disagreement could suggest that the breakdown of turbulence in the interfaces of an exchange flow is not similar to the breakdown in the interface of an arrested saline wedge.

Interfacial Stress in Density Underflow

52. A detailed study of the mechanism of interfacial flow between fresh and saline waters was given by Loftquist (1960). The case considered is the flow of saline water under a stagnant body of fresh water in a horizontal flume. The matters examined relate to the interfacial gradient and stress, entrainment, distribution of density, stress and velocity in a cross section, and relation of the length of transition

layer to the densimetric Froude number. For the present, however, only the results of the coefficient of interfacial resistance will be considered. Loftquist defines the resistance coefficient as

$$\lambda_m = \frac{\tau_m}{\rho u_o^2} \tag{126}$$

where τ_m is in effect the stress of interface and u_o is the maximum velocity of saline waters in a cross section. The densimetric Froude number is defined as

$$F_L = \frac{U^2}{g\left(\frac{\Delta\rho}{\rho}\right) h_r} \tag{127}$$

where h_r is hydraulic radius of the saline water layer

$$h_r = \frac{bh_s}{(b + h_s)} \tag{128}$$

where h_s is the depth of the saline water layer, 2b the width, and U the mean velocity in the cross section of the saline layer. In the experiments conducted, h_s was about 18 or 19 cm and b , 11.5 cm, so that $h_r = 0.37h_s$. The Reynolds number was defined as

$$R_L = \frac{Uh_r}{\nu_s} \tag{129}$$

where ν_s is the viscosity of saline waters. The stress τ_m is deduced from the equation of motion of saline layer making use of observed velocity distribution and the fall of the interface. Evaluations yield for the coefficient of interfacial resistance

$$\lambda_m = 4.34R_L^{-1}\beta_m \tag{130}$$

where β_m is a function of R_L and F_L.
For the purpose of comparing with the findings of the present study, it is desirable to express densimetric Froude number and Reynolds number in term of h_s instead of h_r, thus

$$F_k = \frac{U^2}{g \frac{\Delta\rho}{\rho} h_s} \quad \text{and} \quad R_k = \frac{Uh_s}{\nu} \tag{131}$$

These give

$$F_k = 0.37F_L \; ; \quad R_k = 2.7R_L \tag{132}$$

Following the representation previously used, Equation 97, the coefficient of interfacial friction in terms of mean velocity U

$$\lambda_i = \frac{2\tau_m}{\rho U^2}$$

Comparing with Equation 126

$$\lambda_1 = 2\left(\frac{u_o}{U}\right)^2 \lambda_m$$

During velocity traverses Loftquist found $u_o^2 = 1.21U^2$ so that

$$\lambda_i = 2.42\lambda_m$$

Introducing in Equation 130, λ_m from the last relation and R_L from Equation 132, the result is

$$\lambda_i = 28.5R_k^{-1}\beta_m \tag{133}$$

The dependence of β_m on Reynolds number and densimetric Froude number is given in Figure 17. Construction of the figure is original with us

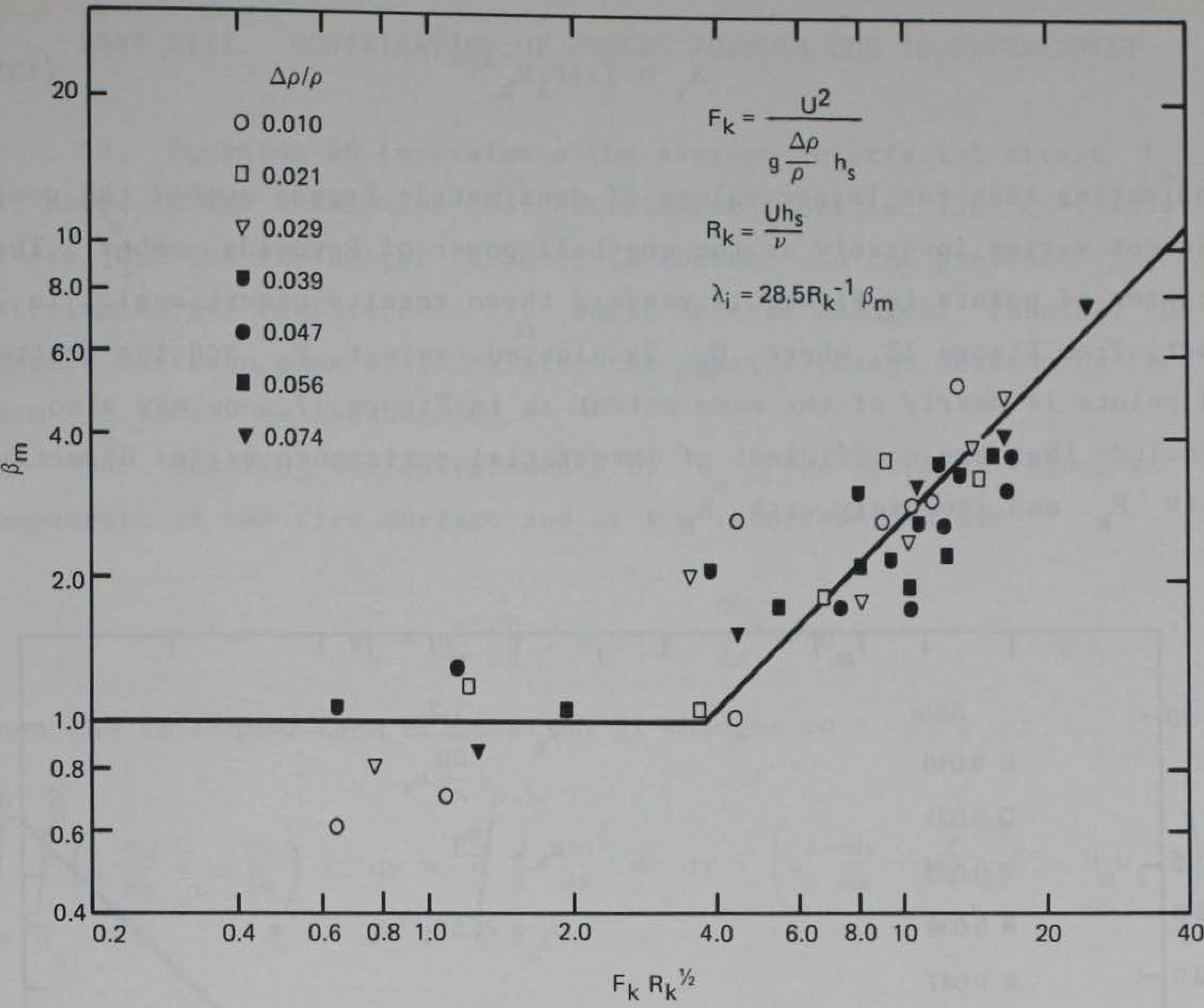

Figure 17. Dependence of β_m on Reynolds and densimetric Froude numbers (after Loftquist 1960)

and is based on data given by Loftquist. When $F_k R_k^{1/2}$ is less than 5, β_m equals unity and in this range the interfacial resistance coefficient is

$$\lambda_i = 28.5 R_k^{-1} \tag{134}$$

a result in close agreement with the findings of the present study, Equation 117. Further in the range $FR^{1/2}$ is greater than 4

$$\beta_m = 0.25 F_k R_k^{1/2}$$

which yields

$$\lambda_i = 7.1 F_k R_k^{-1/2} \tag{135}$$

indicating that for larger values of densimetric Froude number the coefficient varies inversely as the one-half power of Reynolds number. The scatter of points in Figure 17 renders those results provisional. In fact, from Figure 18, where β_m is plotted against F_k and the scatter of points is nearly of the same extent as in Figure 17, one may also conclude that the coefficient of interfacial resistance varies directly with F_k and inversely with R_k.

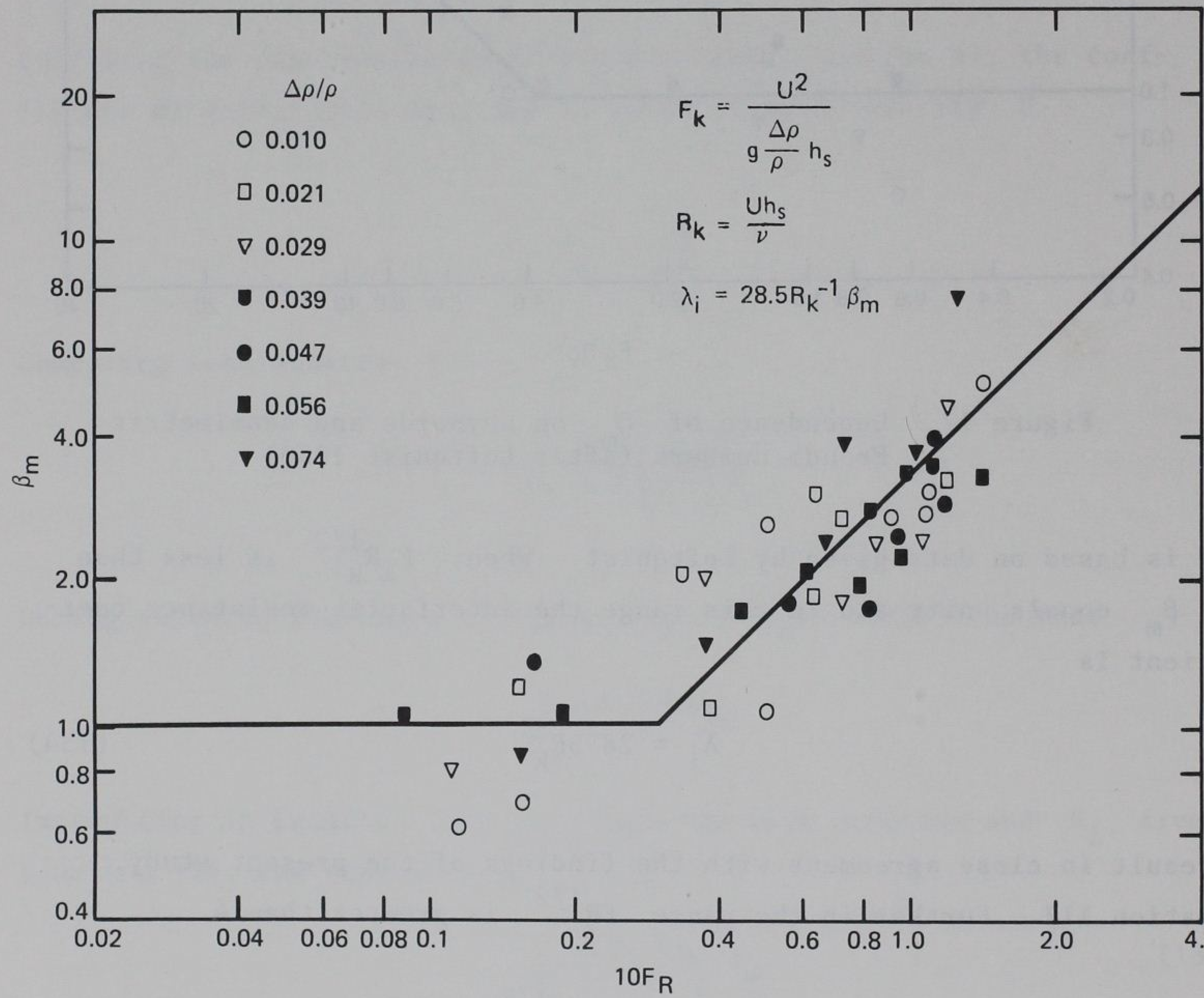

Figure 18. Dependence of β_m on densimetric Froude number (after Loftquist 1960)

PART XIII: MODIFICATION OF STRESS FORMULA DUE TO ENTRAINMENT

53. Equation 66 to evaluate the average interfacial stress T_s was based on the assumption that entrainment (that is, flow of saline waters into the freshwater current) is absent. In the presence of entrainment the coefficients I_n would undergo changes. Possibly the kinetic reaction time will register the greater change leading to the form $I_2 + \delta I_2$ as shown below.

54. Denoting the entrainments by U_m, the vertical velocity components at the free surface and at the interface now are

$$w_s = u_s \frac{dh}{dx} \text{ , } w_i = u_i \frac{dh_s}{dx} + U_m$$

Then the left-hand term of Equation 21 changes to

$$\int_{-b}^{b}\int_{h_s}^{h}\left(u \frac{\partial u}{\partial x} + w \frac{\partial u}{\partial z}\right) dz\ dy = \int_{-b}^{b}\int_{h_s}^{h} \frac{du^2}{dx}\ dz\ dy + \left(u_s^2 \frac{dh}{dx} - u_i^2 \frac{dh_s}{dx} - U_m u_i\ B\right)$$

and in the place of Equation 24 one now has

$$\int_{-b}^{+b} \int_{h_s}^{h} \left(u \frac{\partial u}{\alpha x} + w \frac{\partial u}{\alpha z}\right) dz\ dy = \frac{d}{dx}\ (\alpha U^2 A) - U_m u_i B$$

Integrating the right-hand member between $x = 0$ and $x = x_o$ and dividing by B, the result is

$$\alpha U_1^2 h_{w1} - \alpha U_o^2 H_o - \int_{o}^{x_o} U_m u_i\ dx \qquad (136)$$

where h_{w1} is the depth of fresh water at river mouth, $h_{w1} = H_o - h_{s1}$. In view of condition of continuity

$$U_1 h_{w1} = U_o H_o + \int_o^x U_m \, dx$$

and placing $u_i = mU$, $m = 0.53$, previously noted, and $U_m = kU$ Equation 136 reduces to

$$\alpha U_o^2 H_o \left(\frac{H_o}{h_{w1}} - 1 \right) + 2 \frac{H_o}{h_{w1}} k \int_o^{x_o} UU_o \, dx - mk \int_o^{x_o} U^2 \, dx$$

Dividing by $U_o^2 x_o$

$$\alpha \frac{H_o}{x_o} \left(\frac{H_o}{h_{w1}} - 1 \right) + k \frac{H_o}{x_o} \left[2 \frac{x_o}{h_{w1}} \int_o^1 \left(\frac{U}{U_o} \right) d\zeta - m \frac{x_o}{H_o} \int_o^1 \left(\frac{U}{U_o} \right)^2 d\zeta \right]$$

This may be written as

$$\alpha \frac{H_o}{x_o} I_2 + \frac{H_o}{x} \quad \delta I_2$$

where

$$I_2 = \left(\frac{H_o}{h_{w1}} - 1 \right) = \frac{n}{1 - n} \text{ (as before)}$$

and

$$\delta I_2 = k \left[\frac{2x_o}{h_{w1}} \int_o^1 \left(\frac{U}{U_o} \right) d\zeta - m \frac{x_o}{H_o} \int_o^1 \left(\frac{U}{U_o} \right)^2 d\zeta \right]$$

Hence,

$$\frac{\delta I_2}{I_2} = k \frac{x_o}{H_o} \left[\frac{2}{1 - n} \int_o^1 \left(\frac{U}{U_o}\right) d\zeta - m \int_o^1 \left(\frac{U}{U_o}\right)^2 d\zeta \right] \frac{1 - n}{n}$$

Assuming $n = 0.45$, adapting $m = 0.53$, assigning to U/U_o the value

$$\frac{U}{U_o} = 1 - n \frac{h_s}{h_{s1}}$$

sufficiently accurate for the present purpose and carrying out the required integration using h_s/h_{s1} from Table 4, we find

$$\frac{\delta I_2}{I_2} = 4.46k \frac{x_o}{H_o} \tag{137}$$

In a previous investigation on mixing in arrested saline wedges (Keulegan 1955a), it was shown that

$$U_m = k(U - U_c) \qquad k = 2.12 \times 10^{-4}$$

where U_c is the critical velocity for the initiation of mixing at the interface obeying the relation

$$U_c = 7.3(\nu g \Delta\rho/\rho)^{1/3}$$

In the above analysis U_c was neglected for simplicity. Using k as presently given

$$\frac{\delta I_2}{I_2} = 9.4 \times 10^{-4} \frac{x_o}{H_o} \tag{138}$$

In the tests of the present study x_o/H_o is less than 200. Accordingly, the evaluation of the average interfacial stress T_s on the basis of Equation 66 is nearly correct even if there be mixing at the interface.

55. On the other hand, entrainment across the interface has a much greater effect on the flow pattern in the area of the arrested saline wedge. With entrainment the assumption of similarity in the velocity profiles is no longer valid. Theoretical evaluation of T_o previously made was based on the condition of similarity. The estimated values were found to be inferior to the observed values and this may in part be attributed to the fact that the effect of entrainment was not considered.

PART XIV: NEED FOR FURTHER RESEARCH

56. Expressions of the affine shape of arrested saline wedges and those of relative depth of saline water at the river mouth as established by laboratory observation appear to be equally valid for large rivers. As regards the length of a saline wedge a similar transfer to the prototype condition would not be permissible, especially when the observations are made in narrow channels. One restrictive effect in such channels is the friction of the channel walls. The summary of results from the present and previous investigations was given in Equation 5 for H/B equal to 1 and in Equation 6 for H/B equal to 2. To obtain the corresponding values for infinitely wide laboratory channels one may resort to analysis using the experimentally determined values of the interfacial and bottom stresses (Keulegan 1957b). For a small densimetric Reynolds of the order of 10 thousand

$$\frac{L}{H_o} = 0.22 \left(\frac{V_\Delta H_o}{\nu}\right)^{1/2} \left(\frac{2V_r}{V_\Delta}\right)^{-5/2} \tag{139}$$

and for large densimetric number of order of 10 million

$$\frac{L}{H_o} = 6\left(\frac{V_\Delta H_o}{\nu}\right)^{1/4} \left(\frac{2V_r}{V_\Delta}\right)^{-5/2} \tag{140}$$

The latter should also apply to large rivers if the dependence of the interfacial and bottom stress on Reynolds number is the same as in laboratory small channels. This, however, is certainly open to question.

57. The coefficient of friction of the interface obtained in this study is in agreement with Loftquist data for small velocities of saline waters flowing under a pool of practically stagnant fresh water in a horizontal channel. When mixing is present, Loftquist's data indicate that the coefficient varies as $R^{-1/2}$. This effect is absent in the data of our investigation. The Delft Laboratory tests on exchange flow of lock operation reveal that during initial motion characterized by a

constant densimetric Froude number the coefficient varies as $R^{-1/3}$ for moderately high Reynolds number and eventually at greater high Reynolds numbers above a critical value it remains constant.

58. The direct determination of the stresses, interfacial and bottom, of an arrested wedge is a difficult matter. To reduce the errors due to the side frictions it is desired that new investigation be undertaken with channels of greater width in comparison with water depths. Further, the channels should be of such depth as to allow flows of larger Reynolds number. In addition, closer attention should be paid to the matter of the velocities in the area of the wedge and in cross sections more than one, all uniformly spaced across the length of the wedge. With the larger freshwater velocities the extent of mixing should be determined and its bearing on the wedge area velocities ascertained.

59. If data are available on the saline wedges in large rivers, the question of lengths may be readily examined by assuming that the appropriate relation is

$$\frac{L}{H_o} = A \left(\frac{V_\Delta H_o}{\nu} \right)^n \left(\frac{2V_r}{V_\Delta} \right)^{-5/2} \tag{141}$$

with the constants A and n to be determined. Taking the logarithm of the two sides of the equation, the resulting linear algebraic equation readily yields the values of the unknowns. The procedure certainly should resolve the question if the saline wedge length in rivers is independent of Reynolds number.

REFERENCES

Abraham, G., and Eyesink, W. D. (1971). Magnitude of Interfacial Shear in Exchange Flow, Journal of Hydraulic Research, Vol 9, p. 125.

Barr, D. I. H. (1963). Densimetric Exchange Flow in Rectangular Channels. La Houille Blanche 7, p. 739.

Beta, G. L. 1957. Recirculation of Cooling Water in Rivers and Canals. Proceedings, A.S.C.E., Journal, Hydraulics Division, Vol 83, No. HY3.

Harleman, D. R. F. 1961. Stratified Flow. Section 26, Handbook of Fluid Dynamics, Edit. Streeter, McGraw-Hill, New York.

Ippen, A. T., and D. R. F. Harleman. 1952. Steady State Characteristics of Subsurface Flow, N. B. S. Circular 521.

Keulegan, G. H. 1955b (Aug). Significant Stresses of Arrested Saline Wedges. NBS Report No. 4267, Eight Progress Report on Model Laws for Density Currents. Report to Director, Waterways Experiment Station, Corps of Engineers, Department of Army.

_________. 1957b (Oct). Form Characteristics of Arrested Saline Wedges. NBS Report No. 5482. Eleventh Progress Report on Model Laws for Density Currents. Report to Director, Waterways Experiment Station, Corps of Engineers, Department of Army.

_________. 1949 (Oct). The Determination of Salinities in Tests of Density Currents. NBS Report, Fourth Progress Report on Model Laws for Density Currents. Report to Chief of Engineers, Corps of Engineers, Department of Army.

_________. 1955a (Jun). Interface Mixing in Arrested Saline Wedges NBS Report 4142, Seventh Progress Report to Director, Waterways Experiment Station, Corps of Engineers, Department of Army.

_________. 1957a (Mar). An Experimental Study of the Motion of Saline Water from Locks into Fresh Water Channels. NBS Report 5168, Progress Report on Model Laws of Density Currents, Report to Director, Waterways Experiment Station, Corps of Engineers, Department of Army.

_________. 1952 (Jun). Effectiveness of Salt Barriers in Rivers. NBS Report 1700, Progress Report on Model Laws of Density Currents, Report to Director, Waterways Experiment Station, Corps of Engineers, Department of Army.

Loftquist, K. 1960. Flow and Stress near Interface Between Stratified Liquids, the Physics of Fluids, 3.

Shijf, J. B., and Schoenfeld, J. C. 1953 (Sep). Theoretical Considerations on the Motion of Salt and Fresh Water, Proceedings, Minn. Hyd. Conf., p. 321.

Table 1

Arrested Saline Wedge Observed Data

H_o = 45.5 cm; B = 22.9 cm

No.	U_o , cm/sec	$\Delta\rho$, $\frac{gm}{cm^3}$	h_{s1} , cm	θ ,°C	x_o , cm	ΔH , cm
1B	29.3	0.066	17.44	22.8	2260	1.10
2B	25.6	0.063	19.36	22.8	3230	1.15
3B	23.9	0.068	21.50	22.9	3800	1.08
4B	23.1	0.066	20.90	22.5	4370	1.23
5B	21.3	0.058	22.00	26.6	4730	1.15
6B	20.5	0.067	22.10	23.0	5860	1.22
8B	17.9	0.032	19.50	26.7	2590	0.53
9B	17.0	0.031	20.50	26.0	2870	0.54
10B	16.3	0.031	21.00	25.3	3430	0.56
11B	15.5	0.031	22.50	24.3	4170	0.61
12B	14.4	0.033	22.50	25.4	5040	0.59
13B	14.1	0.030	23.0	25.1	4970	0.59
14B	13.2	0.030	23.75	25.2	5440	0.62
15B	14.1	0.016	18.00	26.0	1680	0.27
17B	12.2	0.015	20.5	26.8	2768	0.30
18B	11.6	0.018	21.0	26.0	3290	0.30
19B	11.0	0.016	21.75	26.2	4680	0.37
20B	10.3	0.016	22.7	25.7	5260	0.33
21B	9.3	0.017	24.0	26.9	5590	0.30

Table 2

Arrested Saline Wedge Observed Data

$H_o = 23.0$ cm; $B = 22.9$ cm

No.	U_o, cm/sec	$\Delta\rho$, $\frac{gm}{cm^3}$	h_{s1}, cm	θ, °C	x_o, cm	ΔH, cm
1	20.1	0.0730	10.0	23.9	1510	0.46
2	18.0	0.0745	10.0	24.0	2776	0.55
3	14.1	0.0730	12.0	24.3	3809	0.52
4	11.7	0.0720	12.7	24.2	5632	0.53
5	14.3	0.0386	9.9	24.4	1130	0.24
6	11.5	0.0368	10.9	24.0	2172	0.24
7	10.0	0.0382	11.1	22.6	2624	0.26
8	10.0	0.0357	11.3	23.6	2577	0.25
9	8.6	0.0362	12.6	23.8	4117	0.25
10	7.8	0.0355	13.0	23.4	4957	0.27
11	10.3	0.0184	9.7	24.0	903	0.11
12	8.2	0.0181	10.7	24.0	1704	0.12
13	7.2	0.0182	11.0	24.5	2339	0.12
14	6.2	0.0178	11.7	24.8	3215	0.12
15	5.1	0.0172	12.6	22.9	4700	0.13
16	4.8	0.0174	13.2	22.8	5860	0.14
17	7.2	0.0092	9.2	22.8	800	0.055
18	5.9	0.0097	10.6	24.5	1541	0.050
19	4.3	0.0089	11.9	24.8	2832	0.058
20	3.7	0.0088	12.8	25.9	3855	0.057
21	3.3	0.0089	13.3	23.7	5270	0.065

Table 3

Depth of Saline Water at River Mouth

(from Keulegan 1957b)

$2V_r/V_\Delta$	h_{s1}/H_o	$2V_r/V_\Delta$	h_{s1}/H_o
0.10	0.815	0.70	0.480
0.15	0.755	0.75	0.460
0.20	0.718	0.80	0.438
0.25	0.686	0.85	0.412
0.30	0.660	0.90	0.402
0.35	0.635	0.95	0.390
0.40	0.608	1.00	0.375
0.45	0.580	1.05	0.355
0.50	0.555	1.10	0.340
0.55	0.538	1.20	0.310
0.60	0.518	1.30	0.285
0.65	0.492	1.40	0.260
		1.50	0.232

Table 4

Affine Shape of Arrested Saline Wedges

(from Keulegan 1957b)

ζ	h_s/h_{s1}	ζ	h_s/h_{s1}
0.00	0.000	0.55	0.500
0.05	0.138	0.60	0.538
0.10	0.189	0.65	0.570
0.15	0.240	0.70	0.608
0.20	0.280	0.75	0.647
0.25	0.318	0.80	0.685
0.30	0.345	0.85	0.748
0.35	0.380	0.90	0.812
0.40	0.410	0.95	0.885
0.45	0.440	1.00	1.000
0.50	0.468		

Table 5

Affine Shape of Arrested Saline Wedges

$H_o = 23.0$ cm; $B = 22.9$ cm; $F_o = 0.40$

$\Delta\rho/\rho$	0.0098	0.0174	0.0396	0.0580	0.0696	
U_o, cm/sec	5.80	7.70	11.9	14.8	18.0	Mean
ζ	h_s/h_{s1}					
0.07	0.000	0.000	0.000	0.000	0.000	0.000
0.05	0.154	0.165	0.137	0.132	0.137	0.145
0.10	0.231	0.231	0.198	0.203	0.187	0.210
0.20	0.330	0.319	0.291	0.286	0.330	0.311
0.30	0.409	0.385	0.368	0.368	0.352	0.376
0.40	0.479	0.434	0.434	0.440	0.418	0.442
0.50	0.547	0.495	0.506	0.506	0.473	0.506
0.60	0.607	0.555	0.577	0.583	0.539	0.572
0.70	0.671	0.621	0.643	0.665	0.605	0.641
0.80	0.742	0.704	0.720	0.748	0.682	0.719
0.90	0.819	0.786	0.786	0.825	0.875	0.799
0.95	0.886	0.863	0.841	0.885	0.847	0.864
1.00	1.000	1.000	1.000	1.000	1.000	1.000

Table 6

Relative Surface Fall over Arrested Salt Wedge

$H_o = 23.0$ cm; $B = 22.9$ cm; $F_o = 0.40$

$\Delta\rho/\rho$	0.0098	0.0174	0.0396	0.0580	0.0696	
U_o, cm/sec	5.80	7.70	11.9	14.8	18.0	Mean
α	h_s/h_{s1}					
0.0	0.000	0.000	0.000	0.000	0.000	0.000
0.1	0.048	0.060	0.060	0.076	0.069	0.063
0.2	0.116	0.121	0.121	0.131	0.141	0.126
0.3	0.184	0.172	0.190	0.174	0.213	0.187
0.4	0.273	0.257	0.281	0.296	0.288	0.280
0.5	0.364	0.336	0.358	0.396	0.313	0.353
0.6	0.465	0.398	0.454	0.500	0.469	0.457
0.7	0.572	0.507	0.557	0.532	0.572	0.548
0.8	0.692	0.618	0.685	0.740	0.656	0.678
0.9	0.835	0.770	0.810	0.870	0.775	0.812
1.0	1.000	1.000	1.000	1.000	1.000	1.000

Table 7

Relative Surface Fall over Arrested Salt Wedge

H_o = 45.5 cm; B = 22.9 cm; F_o = 0.40

$\Delta\rho/\rho$	0.0675	0.0325	0.0172	
U_o, cm/sec	22.8	14.5	10.6	Mean
$\zeta = x/x_o$	$\Delta h/\Delta H$			
0.0	0.000	0.000	0.000	0.000
0.1	0.051	0.053	0.050	0.051
0.2	0.115	0.107	0.102	0.108
0.3	0.176	0.173	0.156	0.166
0.4	0.234	0.287	0.220	0.230
0.5	0.311	0.312	0.288	0.303
0.6	0.412	0.400	0.368	0.394
0.7	0.508	0.504	0.470	0.494
0.8	0.621	0.625	0.592	0.612
0.9	0.770	0.780	0.756	0.766
1.0	1.000	1.000	1.000	1.000

Table 8

Interface Velocities

$H_o = 23.0$ cm; $B = 22.9$ cm; $F_o = 0.40$

$\Delta\rho/\rho$	0.0098	0.0174	0.0396	0.0580	0.0696	
U_o, cm/sec	5.80	7.70	11.9	14.8	18.0	Mean
$\zeta = x/x_o$			U_i/U			
0.1	0.425	0.472	0.413	0.468	0.414	0.438
0.2	0.485	0.508	0.471	0.495	0.452	0.482
0.3	0.527	0.520	0.498	0.509	0.484	0.507
0.4	0.555	0.534	0.519	0.515	0.504	0.525
0.5	0.574	0.541	0.523	0.520	0.516	0.535
0.6	0.594	0.546	0.524	0.523	0.522	0.542
0.7	0.594	0.551	0.522	0.510	0.518	0.539
0.8	0.602	0.550	0.515	0.499	0.511	0.534
0.9	0.609	0.552	0.500	0.485	0.500	0.529
1.0	0.590	0.550	0.475	0.470	0.435	0.502

Table 9

Surface Velocities

H_o = 23.0 cm; B = 22.9 cm; F_o = 0.40

$\Delta\rho/\rho$	0.0098	0.0174	0.0396	0.0580	0.0696	
U_o , cm/sec	5.80	7.70	22.9	14.8	18.0	Mean
$\zeta = x/x_o$	U_s/U					
0.0	1.032	1.043	1.024	1.055	1.048	1.040
0.1	1.042	1.051	1.023	1.060	1.055	1.046
0.2	1.051	1.057	1.030	1.070	1.062	1.054
0.3	1.063	1.065	1.034	1.080	1.060	1.060
0.4	1.072	1.069	1.042	1.080	1.060	1.065
0.5	1.077	1.076	1.050	1.075	1.060	1.066
0.6	1.081	1.078	1.058	1.075	1.058	1.070
0.7	1.084	1.083	1.066	1.070	1.048	1.070
0.8	1.086	1.086	1.073	1.060	1.035	1.068
0.9	1.089	1.090	1.071	1.045	1.020	1.063
1.0	1.091	1.095	1.070	1.035	1.000	1.058

Table 10

Velocity Distribution in Salt Wedge

H_o = 23.0 cm; B = 22.9 cm; F_o = 0.40

Series	1	2	3	4	5	Mean
$\Delta\rho/\rho$	0.0098	0.0174	0.0396	0.0580	0.0696	
h_w, cm	15.1	14.9	15.6	16.4	17.4	15.8
h_s	7.4	7.7	7.1	6.7	6.2	7.0
z'/h_s*	u/U					
0.00	0.540	0.536	0.567	0.480	0.527	0.530
-0.04	0.429	0.406	0.438	0.383	0.406	0.412
-0.08	0.330	0.358	0.351	0.312	0.328	0.336
-0.12	0.257	0.216	0.287	0.258	0.245	0.253
-0.16	0.202	0.163	0.235	0.212	0.184	0.199
-0.20	0.152	0.129	0.195	0.171	0.140	0.157
-0.28	0.060	0.066	0.135	0.109	0.074	0.089
-0.36	-0.040	-0.041	0.072	0.070	0.027	0.018
-0.44	-0.108	-0.086	-0.015	-0.007	-0.042	-0.052
-0.52	-0.148	-0.129	-0.079	-0.081	-0.117	-0.111
-0.64	-0.182	-0.157	-0.135	-0.141	-0.155	-0.154
-0.68	-0.189	-0.161	-0.147	-0.152	-0.160	-0.162
-0.72	-0.192	-0.162	-0.153	-0.156	-0.162	-0.165
-0.76	-0.194	-0.161	-0.154	-0.156	-0.160	-0.165
-0.80	-0.194	-0.159	-0.152	-0.152	-0.155	-0.162
-0.84	-0.191	-0.155	-0.148	-0.143	-0.145	-0.156
-0.90	-0.177	-0.140	-0.132	-0.117	-0.112	-0.136
-0.96	-0.138	-0.103	-0.095	-0.071	-0.062	-0.094
-1.00	0.000	0.000	0.000	0.000	0.000	0.000

* z' is measured from interface upward.

Table 11

Velocity Distribution

in Fresh Water over the Salt Wedge

H_o = 23.0 cm; B = 22.9 cm; F_o = 0.40

Series	1	2	3	4	5	Mean
$\Delta\rho/\rho$	0.0098	0.0174	0.0396	0.0580	0.0696	
h_w , cm	15.1	14.9	15.6	16.4	17.4	15.8
h_s	7.4	7.7	7.1	6.7	6.2	7.0
z'/h*	u/U					
0.00	0.540	0.536	0.567	0.480	0.527	0.530
0.04	0.648	0.666	0.665	0.580	0.646	0.641
0.08	0.736	0.746	0.735	0.651	0.708	0.715
0.12	0.801	0.792	0.785	0.706	0.755	0.768
0.16	0.846	0.827	0.822	0.746	0.789	0.806
0.20	0.880	0.857	0.852	0.780	0.830	0.840
0.24	0.908	0.883	0.876	0.810	0.852	0.866
0.32	0.950	0.921	0.915	0.855	0.886	0.905
0.40	0.982	0.952	0.944	0.889	0.922	0.938
0.56	1.023	0.997	0.987	0.956	0.966	0.986
0.72	1.045	1.026	1.015	1.018	0.994	1.020
1.04	1.062	1.064	1.052	1.056	1.036	1.054
1.20	1.060	1.070	1.064	1.064	1.050	1.062
1.36	1.052	1.072	1.071	1.074	1.062	1.066
1.52	1.040	1.077	1.070	1.080	1.074	1.068
1.68	1.038	1.058	1.064	1.080	1.078	1.060
1.84	1.026	1.046	1.053	1.078	1.078	1.056
2.00	1.011	1.038	1.038	1.072	1.070	1.047
2.32	0.991	1.038	1.021	1.072	1.063	1.037

* z' is measured from interface upward.

Table 12

Evaluation of Total Interfacial and Bottom Frictional Stress Forces

H_o = 23.0 cm; B = 22.9 cm; ν = 0.00919

No.	$\Delta\rho/\rho$	$2V_r/V_\Delta$	h_s/H_o	U_oH_o/ν	$2T_s/\rho U_o^2$	$2T_o/\rho U_o^2$
1	0.0730	1.001	0.370	49.2×10^3	10×10^{-4}	33×10^{-4}
2	0.0745	0.891	0.405	45.2	7	31
3	0.0730	0.698	0.480	35.4	16	22
4	0.0720	0.588	0.523	16.8	20	11
5	0.0386	0.972	0.380	35.9×10^3	19×10^{-4}	30×10^{-4}
6	0.0368	0.806	0.425	28.8	43	32
7	0.0382	0.682	0.485	25.1	56	13
8	0.0357	0.710	0.475	25.1	44	11
9	0.0362	0.601	0.530	21.6	27	27
10	0.0355	0.542	0.540	18.5	48	15
11	0.0184	1.015	0.372	25.8×10^3	20×10^{-4}	43×10^{-4}
12	0.0181	0.773	0.450	21.8	12	68
13	0.0182	0.756	0.455	18.0	48	13
14	0.0172	0.616	0.510	15.4	27	52
15	0.0172	0.523	0.545	12.9	130	26
16	0.0174	0.479	0.570	11.9	38	22
17	0.0092	1.001	0.370	18.1×10^3	56×10^{-4}	50×15^{-4}
18	0.0097	0.803	0.435	14.7	56	41
19	0.0089	0.616	0.510	10.7	56	49
20	0.0088	0.532	0.510	9.3	80	23
21	0.0089	0.472	0.570	8.3	32	24

Table 13

Evaluation of Total Interfacial and Bottom Frictional Stress Forces

H_o = 45.5 cm; B = 22.9 cm; ν = 0.00950

No.	$\Delta\rho/\rho$	$2V_r/V_\Delta$	h_{s1}/H_o	U_oH_o/ν	$2T_s/\rho U_o^2$	$2T_o/\rho U_o^2$
1	0.066	1.08	0.382	14.3×10^4	4×10^{-4}	20×10^{-4}
2	0.063	0.89	0.425	13.7	6	40
3	0.068	0.86	0.472	11.4	6	52
4	0.066	0.85	0.459	11.0	4	20
5	0.058	0.84	0.483	10.2	2	18
6	0.067	0.76	0.485	9.8	6	24
8	0.032	0.95	0.427	8.6×10^4	4×10^{-4}	42×10^{-4}
9	0.031	0.91	0.450	8.2	4	36
10	0.031	0.89	0.461	7.8	2	28
11	0.031	0.87	0.493	7.4	8	32
12	0.033	0.80	0.493	6.9	10	32
13	0.030	0.75	0.502	6.7	16	18
14	0.030	0.76	0.521	6.3	16	16
15	0.016	1.03	0.395	6.7×10^4	4×10^{-4}	30×10^{-4}
17	0.015	0.92	0.450	5.8	16	16
18	0.018	0.80	0.461	5.5	20	28
19	0.016	0.80	0.477	5.3	8	16
20	0.016	0.75	0.498	4.9	12	28
21	0.017	0.65	0.526	4.4	12	60

Table 14

Values of the Definite Integral F_1

n / ε	0.8	0.7	0.6	0.5	0.4	0.3
	F_1					
0.05	4.74	4.94	5.33	5.99	7.07	8.88
0.10	4.26	4.19	4.70	5.25	6.15	7.71
0.15	3.91	3.80	4.25	4.73	5.51	6.88
0.20	3.60	3.46	3.87	4.28	4.97	6.19

Table 15

Values of the Definite Integral F_2

n / ε	0.8	0.7	0.6	0.5	0.4	0.3
	F_2					
0.05	3.95	3.17	2.67	2.39	2.19	2.10
0.10	3.85	3.02	2.57	2.28	2.08	1.98
0.15	3.74	2.91	2.46	2.17	1.97	1.87
0.20	3.63	2.80	2.30	2.06	1.87	1.76

APPENDIX A: NOTATION

b	Half width of channel
B	Width of channel
F_k	Densimetric Froude number $F_k = U^2/\frac{\Delta\rho}{\rho}\ gh_s$ for saline underflow
F_L	Densimetric Froude number $F_L = U^2/\frac{\Delta\rho}{\rho}\ gh_r$ for saline underflow below stagnant fresh water
F_o	Densimetric Froude number $F_o = U_o^2/\frac{\Delta\rho}{\rho}\ gH_o$ arrested saline wedge. $F_o = U_r^2/\ \frac{\Delta\rho}{\rho}\ gH_o$ for lock exchange flow
h	Total depth of water in the area of the arrested wedge
h_r	Hydraulic radius of saline waters of a saline underflow, $h_r = bh_s/(b + h_s)$
h_s	Depth of saline water in an arrested saline wedge; depth of saline water of an underflow or the depth of saline water in a lock exchange flow
h_{s1}	Depth of saline water of an arrested wedge at the river mouth
h_w	Depth of fresh water in the layer over the arrested wedge
h_{w1}	Depth of fresh water at the river mouth
H_o	Depth of fresh water at the tip of an arrested saline wedge; total depth of the fresh and the saline water layers of a lock exchange flow
L	Total length of arrested saline wedge. Same as x_o
M	Momentum of body liquid of arrested saline wedge, and of body of fresh water resting on the entire length of arrested saline wedge
$M_1 + M_o$	Value of M at time t
$M_2 + M_o$	Value of M at time $t + \Delta t$
n	Ratio h_s/h_{s1}
P_i	Pressure total force acting on the entire interface
P_1, P_2	Pressure forces on the upstream and the downstream faces in freshwater layer
Q	Discharge of river waters
R	Reynolds number U_oH_o/ν for arrested wedge

R_e Reynolds number U_2R_2/ν for exchange flow

R_k Reynolds number Uh_s/ν for saline underflow

R_L Reynolds number Uh_r/ν for saline underflow

R_2 Hydraulic radius of lock exchange flow, $h_sB/2(h_s + B)$

T_o Mean bottom stress averaged along the entire length of the arrested saline wedge

T_s Mean interfacial stress averaged along the entire length of the arrested saline wedge

T_{w1} Retarding force from the sidewalls in the entire freshwater layer

T_{w2} Retarding force from the sidewalls in the entire saltwater layer

u Particle velocity; root mean square of velocities in strip plane

u_o Maximum velocity in the saline layer of an underflow

U Mean velocity of fresh water in the layer over an arrested saline wedge; mean velocity of saline water in the layer under the stagnant water of an underflow

U_i Velocity of points at the interface

U_m Velocity of transport across the interface due to mixing

U_o Mean velocity of fresh water at the tip of an arrested saline wedge. Same as V_r

U_r Relative velocity of layers in a lock exchange flow

U_s Velocity of surface waters in an arrested saline wedge

U_1 Mean velocity of fresh water at the river mouth

U_2 Mean velocity of saline layer in a lock exchange flow

V_r River velocity ($V_r = U_o$)

V_Δ Densimetric velocity, $V_\Delta = \sqrt{\frac{\Delta\rho}{\rho} gH_o}$

x Coordinate in the direction of freshwater flow, measured from the tip of an arrested saline wedge

x_o Length of an arrested saline wedge. Same as L

y Coordinate in the channel transverse direction, measured from channel midvertical plane

z,z' Coordinates in the vertical; z measured from the bottom of horizontal channel; z' from the interface

α Boussinesq coefficient of velocity distribution in relation to freshwater flow over arrested saline wedge

β	Boussinesq coefficient in relation to saline waters of arrested wedge
β_m	Numerical factor in Loftquist formula for λ_m
Δ_h	Fall of free surface in the area of an arrested saline wedge
ΔH	Fall of free surface at the river mouth, $H_o = \Delta H + h_{w1} + h_{s1})$
η	Relative depth of salt wedge, h_s/H_o
η_L	Relative depth of salt wedge at river mouth, same as $\eta = h_{s1}/H_o$
θ	Temperature of water expressed in centigrade
ϕ	A function of η defined by Equation 107
λ	Coefficient of resistance of river channel
λ_i	Interfacial coefficient of resistance. $\lambda_i = 2\tau_i/\rho U^2$ for arrested saline wedges and for saline underflow. $\lambda_i = 2\tau_i/\rho U_r^2$ for lock exchange flow
λ_m	Interfacial coefficient of resistance $\lambda_m = \tau_m/\rho U_o^2$ for saline underflow
λ_o	Coefficient of resistance defined by Equation 65
μ	Viscosity of water
ν	Kinematic viscosity of water
ν_s	Kinematic viscosity of saline water
τ_i	Interfacial stress for arrested saline wedge or for lock exchange flow or for underflow
τ_m	Maximum value of stress in underflow, practically same as τ_i
τ_o	Bottom stress of an arrested saline wedge
τ_s	Interfacial stress
$\bar{\tau}_s$	Average value of interfacial stress along the channel width
τ_w	Stress of vertical wall
$\bar{\tau}_w$	Average value of wall stress across span $h - h_s$